



Magnitude, Trends, and Impacts of Ambient Long-Term Ozone Exposure in the United States from 2000-2015

Karl M. Seltzer¹, Drew T. Shindell^{1,2}, Prasad Kasibhatla¹, Christopher S. Malley³

¹Nicholas School of the Environment, Duke University, Durham, NC, USA

5 ²Duke Global Health Initiative, Duke University, Durham, NC, USA

³Stockholm Environmental Institute, Department of Environment and Geography, University of York, York, UK

Correspondence to: Karl M. Seltzer (kms147@duke.edu); Drew T. Shindell (drew.shindell@duke.edu)

Abstract. Long-term exposure to ambient ozone (O₃) is associated with a variety of impacts, including adverse human-health effects and reduced yields in commercial crops. Ground-level O₃ concentrations for assessments are typically predicted using
10 chemical transport models, however such methods often feature biases that can influence impact estimates. Here, we develop and apply artificial neural networks to empirically model long-term O₃ exposure over the continental United States from 2000-2015, and generate a measurement-based assessment of impacts on human-health and crop yields. Notably, we find that two commonly-used human-health averaging metrics, based on separate epidemiological studies, differ in their trends over the study period. The population-weighted, April-September average of the daily 1-hour maximum concentration peaked in 2002 at 55.9
15 ppb and decreased by -0.43 [95% CI: -0.28, -0.57] ppb/yr between 2000-2015, yielding a ~18% decrease in normalized human-health impacts. In contrast, there was little change in the population-weighted, annual average of the maximum daily 8-hour average concentration between 2000-2015, which resulted in a ~5% increase in normalized human-health impacts. In both cases, an aging population structure played a substantial role in modulating these trends. By contrast, all agriculture-weighted crop-loss metrics featured decreasing trends, leading to reductions in the estimated national relative yield loss ranging from 1.7-1.9 %
20 for maize, 5.1-7.1% for soybeans, and 2.7% for wheat. Overall, these results provide a measurement-based estimate of long-term O₃ exposure over the United States, quantify the historical magnitude, trends, and impacts of such exposure, and illustrate how different conclusions regarding historical impacts can be made through the use of varying metrics.

1 Introduction

Tropospheric ozone (O₃) is a secondary pollutant that is photochemically formed from precursor gases. Exposure to ambient O₃
25 is associated with adverse health effects in humans (U.S. EPA 2013) and reduced yields in commercial crops (Chameides et al., 1994; Mauzerall and Wang, 2001). These impacts have driven efforts to reduce ground-level O₃ in the United States, specifically targeting peak levels of O₃ concentrations through regulations that control anthropogenic precursor emissions, such as nitrogen oxides (NO_x) and volatile organic compounds (VOCs). These efforts have been widely successful in reducing peak concentrations (Simon et al., 2015; Lefohn et al., 2017; Fleming et al., 2018), but impacts related to both human-health and crop
30 yields nonetheless persist (Cohen et al., 2017; Seltzer et al., 2018; Zhang et al., 2018; Shindell et al., 2019).

Quantifying impacts requires an estimate of human and vegetation exposure to O₃, which is most commonly accomplished through the use of chemical transport models (CTMs; e.g. Anenberg et al. 2010; Silva et al. 2013; Lelieveld et al. 2015; Malley et al. 2017; Shindell et al. 2018, Stanaway et al., 2018). CTMs apply state-of-science knowledge to simulate O₃ formation, termination, and transport, while also providing complete spatial and temporal coverage over a particular domain - a desired trait
35 for impact assessments. However, estimates of exposure and impacts can vary substantially across CTM studies. For example, two CTM based studies estimated 2005 respiratory related premature mortalities in the USA using the same relative risk function



(Jerrett et al., 2009), yet yielded results that differed by $\sim 3\times$ (i.e. 13,000 vs. 38,000; Zhang et al., 2018; Lelieveld et al., 2013). While CTMs accurately reproduce many features of atmospheric chemistry (Shindell et al., 2013; Hu et al., 2018), one important issue associated with CTM-based impact assessments is that CTMs are consistently high biased when predicting O₃ exposure-relevant concentrations (Schnell et al., 2015; Travis et al., 2016; Yan et al., 2016; Seltzer et al., 2017; Porter et al., 2017; Guo et al., 2018). Such biases can influence estimates of impacts and are often amplified by nonlinear concentration-response functions (Seltzer et al., 2018). Measurement-based methods, including area-weighted average of nearby monitors, nearest monitor, inverse distance weighting, Kriging interpolation, and multiple-linear regression under a Bayesian framework, can also be used to estimate exposure (Bell, 2006; Brauer et al., 2008; Marshall et al., 2008; Chang et al., 2010; Seltzer et al., 2018). However, a notable limitation of such methods stems from the sparse spatial coverage of monitoring sites. While these limitations might be minor in areas with dense monitoring, such methods can become insufficient as the distance from monitors increases (Bell, 2006).

O₃ exposure trends are also of great interest to researchers and air quality managers. To accurately model trends of O₃ exposure, many dimensions of variability must be captured. For the annual average of the maximum daily 8-hour average O₃ concentration (hereafter MDA8), a metric used to quantify long-term O₃ exposure in epidemiological studies (e.g. Turner et al., 2016; Lim et al., 2019), the O₃ diurnal and seasonal cycles must be accurately simulated over time. CTM evaluation studies also report the existence of seasonal, spatial, and diurnal variability in model performance (Cooper et al., 2014; Schnell et al., 2015; Seltzer et al., 2017; Lin et al., 2017; Guo et al., 2018; Strode et al., 2019; Young et al., 2018). These variances can lead to conflicting conclusions regarding trends in exposure. Zhang et al., 2018 report a $\sim 9\%$ decrease in the population-weighted, daily maximum 1-hour exposure concentration of O₃ in the USA warm-season between 1990-2010. Meanwhile, a separate study reported no change in the population-weighted, daily maximum 8-hour exposure concentration of warm-season O₃ over those two decades (Stanaway et al., 2018).

Since monitoring data is sparse, quantification of trends using observations requires either continuous, long-term measurement data at a particular site or the aggregation of observations into regions (e.g. Southeast, Northeast, Great Plains, etc.) and/or urban-rural-suburban classifications. Many studies have indeed made use of such data to assess O₃ trends (Jaffe and Ray, 2007; Cooper et al., 2012; Parrish et al., 2012; Cooper et al., 2014; Simon et al., 2015). The recent publication of the Tropospheric Ozone Assessment Report (TOAR) database (Schultz et al., 2017) has created a rich observational dataset and further expanded the number of such assessments (e.g. Chang et al., 2017; Gaudel et al., 2018; Lefohn et al., 2018; Fleming et al., 2018; Mills et al., 2018b).

In this study, we use artificial neural networks (ANNs) and the TOAR database to estimate a suite of O₃ impact metrics related to human-health and crop yield over the contiguous United States from 2000-2015 at $0.5^\circ \times 0.5^\circ$ resolution. Specifically, we take advantage of the improved long-term coverage afforded by the TOAR database to develop a framework that empirically estimates O₃ exposure with complete spatial and temporal coverage over the United States. ANNs have been previously used to make O₃ predictions (Ruiz-Suárez et al., 1995; Yi and Prybutok, 1996; Comrie, 1997; Gardner and Dorling, 2000; Dutot et al., 2007; Di et al., 2017), but generally at the monitor or city level. Our main goal was to better quantify the magnitude and trends of population-weighted and agriculture-weighted long-term (i.e. months, annual) O₃ exposure in the USA over many consecutive years, and use those estimates to generate a measurement-based assessment of impacts and trends on human-health and crop yields. In addition, we applied the ANN to meteorologically adjust exposure predictions, thus eliminating a substantial proportion of the short-term variability and enabling a better quantification of long-term O₃ exposure trends.



75 2 Methods

2.1 Observational Dataset and Impact Metrics

Daily O₃ observations spanning 2000-2015 from the Airmap, AQS, CAPMoN, CASTNET, GAW, and NAPS monitoring networks in North America were retrieved from the TOAR database (Schultz et al., 2017). These daily observations were used to calculate two human-health and two crop-yield relevant averaging metrics. The first human-health metric comes from the Jerrett et al. (2009), hereafter J2009, long-term O₃ exposure epidemiology study. Using data from the American Cancer Society Cancer Prevention Study II (ACS CPS-II) cohort, J2009 estimated changes in cause-specific mortalities attributable to incremental changes in the April-September average of the daily 1-hour maximum O₃ concentration (hereafter MDA1). The second human-health metric is from the Turner et al. (2016), hereafter T2016, long-term O₃ exposure epidemiology study. T2016, using an expanded version of the ACS CPS-II cohort that included more follow-up years, a larger population, and more events (i.e. deaths), reported changes in cause-specific mortalities attributable to incremental changes in the annual average of the maximum daily 8-hour average O₃ concentration (hereafter MDA8). To elucidate the influence of the underlying seasonal trends on the MDA8 metric, we subdivide this annual metric into 3-month seasonal windows (i.e. summer: June-August; spring: March-May). These seasonal divisions will be labeled as such: MDA8-MAM (spring), MDA8-JJA (summer), MDA8-SON (fall), and MDA8-DJF (winter).

The two crop-loss metrics included here were the M12 and AOT40 averaging metrics. Both have been used in a variety of crop loss assessments (e.g. Van Dingenen et al., 2009; Avnery et al., 2011; Shindell et al., 2019). The M12 metric, which can be used to calculate impacts on maize and soybean relative-yields, is defined as the mean O₃ value for the local hours of 8:00-20:00, averaged over the 3-months prior to the start of the harvest period. The AOT40 metric, which can be used to calculate impacts on maize, soybeans, and wheat, is an accumulative index and defined as a summation of the hourly mean O₃ values over 40 ppb for the local hours of 8:00-20:00, also averaged over the 3-months prior to the start of the harvest period. We initialize the start of the harvest period to be consistent with Avnery et al. (2011). For maize and soybeans, the 3-month averaging period was initialized in July. Wheat features two varieties with separate initialization months for harvesting. One is initialized in March and the other is initialized in May. Exposure results of both varieties are included for illustrative and seasonal comparisons. It should be noted that long-term O₃ exposure also stunts the yields of a variety of other crops, such as rice (Van Dingenen et al., 2009; Shindell et al., 2019), but inclusion of these impacts were not considered here since they are not a major commercial crop in the United States.

2.2 Artificial Neural Network

We utilized feed-forward ANNs, also referred to as multilayer perceptrons (MLPs), to model the four metrics considered here, with a unique network for each metric. MLPs were constructed using the Keras API (keras.io; Chollet, 2015) and TensorFlow machine-learning library (tensorflow.org; Abadi et al., 2015). Broadly, ANNs consist of several interconnected layers, beginning with an input data layer, ending with an output data layer, and having at least one ‘hidden’ layer between the input and output that models the nonlinear relationships of the system. Each layer is connected via a set of coefficients at individual ‘nodes’ that are optimized through model training, similar to a multiple-linear regression (MLR) model. In contrast to a MLR, a layer in an ANN may have multiple nodes, and the output from each node proceeds through an ‘activation function.’ An activation function can take many shapes, but the two most common are a sigmoidal function (which converts the node output to a probability) and a rectified linear (ReLU) function (which applies a threshold to a linear function). The ANNs used here consisted of one input, three hidden, and one output layer. All nodes in each hidden layers featured a ReLU activation function, including the output



layer to ensure all predictions were non-negative. The three hidden layers, each of which included a bias term, consisted of 32 nodes each.

115 Daily observations from the TOAR dataset spanning 2000-2015 were paired with MERRA-2 meteorological reanalysis data, anthropogenic emissions data from the Community Emissions Data System (CEDS; Hoesly et al., 2018) inventory, and monthly methane concentrations. Meteorological variables that were considered O_3 covariates largely follow Li et al. (2019) and include 24-hour average of cloud area fraction (%), 12-hour average of 2-meter air temperature (K), 24-hour average of 10-meter eastward wind speed (m/s), 24-hour average of 10-meter northward wind speed (m/s), 12-hour average of the planetary boundary

120 layer height (m), total daily precipitation flux ($kg/m^2/day$), 24-hour average of the sea-level pressure (Pa), 12-hour average of the 2-meter specific humidity (kg/kg), 24-hour average of the leaf area index (%), and the 12-hour average of the surface incoming shortwave radiation flux (W/m^2). All 24-hour periods and 12-hour periods (8:00-20:00) were adjusted to local times. Localized anthropogenic emissions included nitrogen oxides (NO_x), non-methane volatile organic carbon (NMVOC; includes total weight of all species), and carbon monoxide (CO). Since emissions from East Asia have a large impact on North American ground-level

125 O_3 concentrations (Liang et al., 2018), and since emissions in the region have dramatically changed in recent decades (Zheng et al., 2018), monthly total emissions from all East Asian countries (i.e. China, Japan, South Korea, North Korea, and Mongolia) were included as an input. Emissions from all East Asian countries were retrieved from the CEDS inventory, with the exception of Chinese emissions, which were retrieved from the Multi-resolution Emission Inventory for China (MEIC) inventory (Zheng et al., 2018). Since the last year included in the CEDS inventory is 2014, anthropogenic emissions for 2014 were repeated for 2015.

130 To incorporate geographical differences and long-term drivers not included as input, several fixed effect variables were also used as input, including latitude, longitude, and year. We normalized all input data by subtracting the mean and dividing by the standard deviation of the training dataset.

Prior to model training, the complete dataset was divided into three components – training, validation, and testing. The training dataset is used to iteratively tune the coefficients in the ANN, the validation dataset is used to ensure the training process does

135 not over fit the ANN parameters to match the training dataset, and the testing dataset is used to evaluate how well the trained model performs. To compile these components, all available data in a given month was collected and three random, consecutive days were removed for validation and four random, consecutive days were removed for testing. The remaining days became the training dataset. In total, the size of the training data set eclipsed five million values; therefore, the number of trainable parameters was nearly 4-orders of magnitude smaller. The optimization of all coefficients at each node in the ANN is

140 accomplished through stochastic gradient descent (SGD) optimization. SGD consists of (a) taking mini batches of the training dataset, (b) estimating the gradient of all coefficients relative to the known output, (c) taking a small iterative step towards optimal solution, (d) repeating with a new mini-batch of the training dataset, and (e) repeating steps (a)-(d) until the entire training dataset has been fed through the network. The set of steps (a)-(e) is referred to as an epoch, and network training proceeds through multiple epochs. In total, we used the Adam Optimizer (Kingma and Ba, 2015), with a learning rate of 0.001

145 (i.e. the size of step (c)), a decay factor of 0.9 (i.e. a shrinking of the step (c) size), and a mean-squared error target cost-function. Each ANN was trained for 3,000 epochs, with a shuffling of the training data between each epoch. Through monitoring of the model training, it was determined that 3,000 epochs was sufficient to optimize the system without over fitting.

To quantify the added benefit of the ANN over a simplified model, a comparison with results from a MLR is included. In addition, since exposure mostly occurs at unobserved locations, and all of the model training explained thus far is only evaluated

150 at observed locations (i.e. via the testing dataset), we added an additional step to test our methods. In short, we performed several CTM simulations and sampled the daily-level CTM predictions of each metric at all available monitoring locations. We then followed the same machine learning process described above, except using the CTM's pseudo-observational dataset and four



newly trained ANNs, to predict the population-weighted (MDA1/MDA8) and agriculture-weighted (M12/AOT40) exposure values estimated by the CTM. Through this process, we can assess the network's ability to predict total exposure through the exclusive use of sparse measurements.

2.3 Chemical-Transport Modeling

The CTM pseudo-observational dataset of ground-level O₃ was generated using GEOS-Chem (v11-01; <http://www.geos-chem.org>; Bey et al., 2001). A nested version of the model at 0.5° x 0.625° horizontal resolution, driven by native resolution MERRA-2 meteorology and fed annually varying 2.0° x 2.5° boundary conditions, was utilized to simulate O₃ throughout the continental United States for the years 2000, 2003, 2005, 2007, 2010, 2012, and 2014. The model includes comprehensive HO_x-NO_x-VOC-O_x gas chemistry, coupled to an aerosol module that includes sulfate-nitrate-ammonium chemistry (Park et al., 2004; Pye et al., 2009), primary carbonaceous aerosols (Park et al., 2003), mineral dust (Fairlie et al., 2007), and sea salt (Jaegle et al., 2011), with aerosol thermodynamics simulated using ISORROPIA II (Fountoukis & Nenes, 2007). Global anthropogenic emissions come from the CEDS inventory (Hoesly et al., 2018) and are processed through the Harvard NASA Emission Component (HEMCO; Keller et al., 2014). All nested simulations featured a 2-month spin-up, each O₃ metric is calculated at local time, and ground-level concentrations (10-m) from the first level of the GEOS-Chem output were calculated using the scaling method outlined in Zhang et al. (2012).

2.4 Calculation of Metric Trends

Trends of all metrics are presented both spatially and weighted towards the impact subject of interest (i.e. population-weighted or agriculture-weighted). All trends are assessed at the annual time-scale (i.e. one data point, either grid cell or a population/agriculture-weighted value) using a linear least-squares regression. To calculate population-weighted exposure concentrations, we use population data from the 2017 revisions to the UN Population Division (<https://esa.un.org/unpd/wpp/DataQuery/>), distributed to grid cells using population density data from the Gridded Population of the World (GPW) version 4 (CIESIN 2016). Agriculture-weighted exposure concentrations were calculated using crop production data from the Food and Agricultural Organization data sets (FAO, 2010).

We also account for short-term variability in metric trends by modeling meteorologically adjusted predictions of each metric. To evaluate the ANNs ability to complete this task, we performed CTM simulations of 2003, 2005, 2007, 2010, 2012, and 2014 using meteorological conditions from each respective year, but frozen anthropogenic emissions and methane concentrations from 2000. We then used the previously trained ANNs (i.e. the ANNs generated using the CTM pseudo-observational data) to predict the population-weighted and agriculture-weighted exposure metrics from these CTM sensitivity simulations. Finally, we compared the CTM and ANN predicted trends attributed to meteorology between 2000-2015. This evaluation enables us to evaluate how well the ANN can estimate meteorologically adjusted exposure trends. We then applied this framework to the ANNs trained with the TOAR data to estimate meteorologically adjusted trends of the population-weighted and agriculture-weighted exposure metrics.

2.5 Calculation of Human-Health and Crop-Yield Impacts

Human-health impacts were quantified using the exposure-response relationships and averaging metrics reported by J2009 and T2016. Both epidemiological studies found a significant relationship between exposure to long-term O₃ and premature respiratory mortality. Respiratory impacts are the lone end-point considered here since it is the most common impact considered by the community. However, it should be noted that T2016, as well several other studies (Jerrett et al., 2013; Crouse et al., 2015;



190 Cakmak et al., 2016; Lim et al., 2019), found a significant relationship between long-term O₃ exposure and other mortality end points, such as cardiovascular disease.

Impact assessments for human-health generally report results in terms of the estimated number of premature mortalities attributable to long-term exposure. However, these results can often be driven by non-exposure variables, such as changes in population count (Cohen et al., 2017), baseline mortality rates (Cohen et al., 2017), and population aging (Apte et al., 2018). To
195 eliminate the influence of changes in the total population count on net impacts, we normalize our results and report estimated health impacts as premature mortalities per 100,000 people attributable to long-term O₃ exposure. We then illustrate the percent contributions of each remaining variable (i.e. population aging, changes in baseline mortality rates, and exposure) on the net health impact calculations.

Normalized premature mortalities attributable to long-term O₃ exposure were calculated as follows:

$$200 \quad \Delta X = \begin{cases} 0 & \text{if } [O_3] \leq TMREL \\ [O_3] - TMREL & \text{if } [O_3] > TMREL \end{cases} \quad (1)$$

$$HR = \exp^{\beta \Delta Y} \quad (2)$$

$$AF = 1 - \exp^{-\beta \Delta X} \quad (3)$$

$$\Delta Mort_i = y_{0i} \times AF \times Population_i \quad (4)$$

$$Normalized \ Mort = \left(\frac{\sum_{i=1}^n \Delta Mort_i}{\sum_{i=1}^n Population_i} \right) \times 100,000 \quad (5)$$

205 Where TMREL is the theoretical minimum risk exposure level, ΔX is the predicted long-term O₃ exposure concentration above the TMREL, β is the exposure-response factor, HR is the hazard ratio reported by the epidemiological study, ΔY is 10 ppb in both epidemiological studies, AF is the attributable fraction of the disease burden attributable to long-term O₃ exposure, y_0 is the cause-specific, age-binned baseline mortality rate, Population is the age-binned population count, i is the age-bin index, $\Delta Mort$ is the estimated number of cause-specific, age-binned premature mortalities, n is the number of age-bins, and Normalized Mort is
210 the estimated number of cause-specific premature mortalities per 100,000 people attributable to long-term O₃ exposure. Baseline mortality rates were derived by the 2017 GBD project (Stanaway et al., 2018) and mapped to best match the ICD-10 codes reported in T2016. The hazard ratio for respiratory diseases was 1.040 (95% CI: 1.013, 1.067) and 1.12 (95% CI: 1.08, 1.16) in J2009 and T2016, respectively. The TMREL's used were 33.3 ppb when using the J2009 averaging metric and 26.7 ppb when using the T2016 averaging metric.

215 We report agriculture (maize, soybean, and wheat) impacts in terms of a national relative yield loss (RYL) due to long-term O₃ exposure. We follow the concentration-response function and RYL methods outlined in Van Dingenen et al. (2009), as summarized below.

$$Maize \ RYL \ [M12] = 1 - \left(\frac{\exp \left[- \left(\frac{M12}{124} \right)^{2.83} \right]}{\exp \left[- \left(\frac{20}{124} \right)^{2.83} \right]} \right) \quad (6)$$

$$Soybean \ RYL \ [M12] = 1 - \left(\frac{\exp \left[- \left(\frac{M12}{107} \right)^{1.58} \right]}{\exp \left[- \left(\frac{20}{107} \right)^{1.58} \right]} \right) \quad (7)$$

$$220 \quad Maize \ RYL \ [AOT40] = AOT40 \times 0.00356 \quad (8)$$

$$Soybean \ RYL \ [AOT40] = AOT40 \times 0.0113 \quad (9)$$

$$Wheat \ RYL \ [AOT40] = AOT40 \times 0.0163 \quad (10)$$

3 Results

3.1 Artificial Neural Network Training and Evaluation

225 To test the methods employed in this analysis, we first sampled daily GEOS-Chem output at all available monitoring locations to



generate a CTM pseudo-observational dataset. We then used this dataset to train four ANNs (i.e. one for each metric) and attempted to recreate the original GEOS-Chem output. Through this process, we attempt to determine the strength of an ANN in reconstructing complete exposure maps using sparse observation data. The RMSE results from the training and validation datasets are similar (Table 1), indicating that the network is not over fitting and is generalizing the system well. When compared to a MLR, the RMSE testing results are ~33% lower, demonstrating the added benefit of the ANN (Table 1). Population-weighted and agriculture-weighted exposure estimates from the ANN closely match the predictions from GEOS-Chem (red vs. blue in Fig. 1) for all metrics. An exception is the marginal high bias of the AOT40 metrics for wheat early in the time series. Overall, the ANN is able to reproduce the complete exposure predictions with high fidelity, as estimated by GEOS-Chem, using information strictly from monitoring locations. We also find that the ANN generally performs well when meteorologically adjusting the predicted exposure trends (i.e. the short-term variability and trends attributable to meteorology; green vs. yellow lines in Fig. 1). The small deviations, again largely confined to the AOT40 metrics, are due to a few factors. First, regions of dense agriculture production are limited and generally located in areas with fewer monitors, limiting the extent of model training. Second, the AOT40 metric is an accumulation index, leading to the amplification of small biases.

With confidence in the overall framework, we then trained new ANN's using daily 2000-2015 observations from the TOAR database. Little difference between the training, validation, and testing performance metrics indicate that each ANN was not over fit (Table 2). In addition, we again find the ANN performs ~30% better than a MLR model (Table 2). When compared to the original TOAR database, we find high accuracy between each ANN predicted long-term metric and the original observations (Figs. S1-S4; Table S1). The RMSE of the MDA1 and MDA8 predictions ranged from 3.1 – 4.4 ppb and 2.3 – 3.9 ppb, respectively (Table S1). The r^2 of the two metrics ranged from 0.77 – 0.84 and 0.74 – 0.82, respectively. Similar levels of bias (RMSE) and correlation (r^2) were found when comparing the long-term agriculture metrics (Table S1).

3.2 Magnitude and Trends of Long-Term O₃ Exposure Metrics

3.2.1 Human-Health Relevant Metrics

The MDA1 metric featured large reductions throughout the study period, with downward trends exceeding 1 ppb/yr in the Southeast and in large portions of California (Fig. 2). As a result, exposure throughout this period simultaneously decreased. The national population-weighted exposure concentration peaked in 2002 at 55.9 ppb, reached a minimum of 48.2 ppb in 2014, and featured sizeable year-to-year fluctuations due to inter-annual variation (Fig. 3). From 2000-2015, the population-weighted exposure concentration of the MDA1 metric featured a national annual decrease of -0.43 [95% CI: -0.28, -0.57] ppb/yr. After adjusting for meteorology, the trend changes to -0.41 [95% CI: -0.35, -0.47] ppb/yr. The similar mean values of these two trends suggest that nearly all of the MDA1 reductions are due to non-meteorological drivers (i.e. emission changes, intercontinental transport, methane, etc.). Changes in exposure also featured an east-west divide, with population-weighted exposure concentrations decreasing by -0.49 [95% CI: -0.28, -0.69] ppb/yr in the east and -0.31 [95% CI: -0.21, -0.41] ppb/yr in the west (Fig. 3, Table S4).

In contrast, the MDA8 metric featured more modest decreases in the Southeast USA and scattered areas with increasing trends (Fig. 2). This divergence between the two human-health metrics is due to the different averaging periods (i.e. the traditional 'ozone-season' vs. an annual average). If only summer months were considered when calculating the MDA8 metric (i.e. MDA8-JJA), the two trends would be spatially and quantitatively consistent (Fig. 2). However, O₃ increases during the winter months (i.e. MDA8-DJF) partially compensate for the summer decreases, resulting in no discernable trend for the national population-weighted MDA8 metric (Fig. 3). After adjusting for meteorology, the national population-weighted MDA8 trend from 2000-2015 is -0.02 [95% CI: 0.01, -0.04] ppb/yr (Fig. 3). Again, trends featured an east-west divide. While only marginally different,



265 it is interesting to note that the western MDA8 trends were slightly positive and the eastern MDA8 trends were slightly negative. Prior studies (e.g. Bloomer et al., 2010; Cooper et al., 2012; Parrish et al., 2012; Clifton et al., 2014; Simon et al., 2015; Strode et al., 2015; Fleming et al., 2018) have highlighted the existence of a seasonal shift in the distribution of O₃ concentrations throughout the United States during this century. We find that these shifts have not only manifested in contrasting seasonal trends (i.e. summer decreases vs. winter increases), but have also led to a change in the dominant months of O₃ exposure. For
270 example, the population-weighted exposure concentrations during the spring and summer months (MDA8-MAM vs. MDA8-JJA) were nearly equivalent from 2013-2015 (Table S2).

It should be noted that comparing previously reported seasonal trends of O₃ is difficult due to varying study periods, averaging metrics, and selection of monitoring networks. Oftentimes, rural locations are selected, enabling the isolation of trends in background O₃ concentrations or to minimize the influence of nearby changes in anthropogenic emissions (e.g. Jaffe and Ray,
275 2007; Cooper et al., 2012; Jaffe et al., 2018). For this study, since our focus is on changes in exposure, we incorporate all available observational data, including data from monitors in urban cores. As such, the conclusions regarding O₃ trends can be different.

Cooper et al., 2012, using rural monitoring data spanning 1990-2010, reported a -0.45 ppb/yr and a +0.10 ppb/yr trend in daytime O₃ during summer months for the eastern and western USA, respectively. Though, both trends featured wide ranges. Jaffe et al.,
280 2018, using a limited number of high elevation, rural monitoring sites, reported decreasing trends of median summertime O₃ between 2000-2016 at most analysed locations, with stronger decreases in the east than west (~1 ppb/yr vs. ~0.5 ppb/yr). Lin et al., 2017 also used rural monitoring data, but increased the coverage to include 1988-2014 and found a 0.4-0.8 ppb/yr decreasing trend of median MDA8-JJA concentrations in the eastern USA, and mixed trends in the west. Fleming et al., 2018 take a more exposure-based perspective by incorporating both urban and non-urban monitors and show that the observed magnitude of
285 several warm season human-health ozone metrics are similar for North American urban and non-urban sites, and that the trends are only slightly smaller for the urban areas. We also find a dramatic divide between east and west summertime O₃ exposure trends, but our results differ from some of the prior studies. Our exposure focused estimates of eastern USA trends are similar to the mean reported by Cooper et al., 2012 and on the low end reported by Lin et al., 2017. We also find a consistent decreasing trend in western MDA8-JJA exposure, as well as smaller levels of trend uncertainty (Table S4).

290 Cooper et al., 2012 also report a uniform east and west increase in rural wintertime O₃ concentrations of 0.12 ppb/yr. However, the exclusive selection of rural monitors precludes the extrapolation of those results to estimate exposure trends. This is well illustrated by Simon et al., 2015, who used an extensive network of 1998-2013 observations to show that there is a strong rural-urban divide in mean winter O₃ trends, with increasing trends more prevalent in urban areas. Indeed, when compared to Cooper et al., 2012, we find a much stronger trend increase in MDA8-DJF exposure (Table S4). While we do find a near uniform
295 increase in east and west MDA8-DJF population-weighted concentrations, our results indicate that the national trend in MDA8-DJF exposure was +0.33 [95% CI: 0.37, 0.28] ppb/yr.

3.2.2 Crop-Loss Relevant Metrics

Since the averaging months for crop-loss metrics are dependent on crop variety, the magnitude and trends can feature distinct patterns. All maize and soybean metrics envelop the months of July-September. As such, and consistent with the MDA1 results,
300 this averaging period yields decreases for both the M12 and AOT40 metrics, with the strongest reductions in the southeast and California (Fig. 4, top panels). However, both of these crops are predominantly grown in the Midwest and Great Plains (Fig. S7). These are regions that generally experienced smaller trend reductions. Nationally, the agriculture-weighted trends of the M12 metric for maize and soybeans were -0.35 [95% CI: -0.17, -0.54] ppb/yr and -0.39 [95% CI: -0.19, -0.59] ppb/yr (Table S4). The



agriculture-weighted trends of the AOT40 metric for maize and soybeans were -0.35 [95% CI: -0.18, -0.51] ppmh/yr and -0.39
305 [95% CI: -0.21, -0.56] ppmh/yr. After adjusting for meteorology, the mean trend for both metric and crop pairings was reduced
marginally, suggesting that meteorological factors played a role in the net trends from 2000-2015 (Fig. 5).

Both agriculture-weighted AOT40 averaging periods for wheat (MAM and MJJ) featured decreasing, but considerably different,
trends (Fig. 5, bottom right). These trend differences again highlight the seasonal shift in O₃ concentrations. From 2000-2006,
the AOT40-MJJ wheat metric was ~40-60% higher than the AOT40-MAM wheat metric (Table S3). By 2014, both metrics were
310 nearly equal (~5.5-7.0 ppmh). This convergence is also amplified by the 40 ppb threshold applied in the AOT40 calculation.
Towards the end of the study period, daytime O₃ concentrations were reaching 40 ppb in the Midwest and Great Plains (Fig. S3),
thus minimizing the metric's accumulation and causing the two metrics to intersect.

We posit that the influence of meteorology on the agriculture-weighted trends, as indicated by the marginal difference in the
mean and meteorologically adjusted trends, is due to two factors. Prior analysis has shown that two important meteorological
315 variables influencing O₃ include temperature and humidity (Camalier et al., 2007; Jacob and Winner, 2009). The temperature-O₃
mechanism is a function of promoting peroxyacetyl nitrate decomposition (leading to ozone increases near NO_x source regions,
but decreases in remote areas; Doherty et al., 2013) and increases in isoprene emissions. The humidity-O₃ mechanism is a
function of increased water vapor concentrations, which promotes O₃ chemical destruction. According to the MERRA-2
reanalysis product, the Midwest and Great Plains regions featured both decreasing trends in daytime 2-meter temperature and
320 increasing trends in daytime 2-meter specific humidity (Fig. 6). We also propose that the 40 ppb threshold for the AOT40 metric
promotes a disproportionate influence of meteorological variability on its magnitude. This is due to the sensitivity of particular
meteorological variables on extreme O₃ episodes (Russell et al., 2016; Fix et al., 2018).

3.3 Estimates of Long-Term O₃ Exposure Impacts

3.3.1 Human-Health

325 Human-health impacts, reported as the estimated number of premature respiratory mortalities attributable to long-term O₃
exposure per 100,000 people, were strongly dependent on the choice of exposure-response relationship and featured several
differences (Fig. 7). First, the T2016 results reported nearly double the estimated human-health impacts attributable to long-term
O₃ exposure. For example, in 2010, the J2009 and T2016 estimated impacts were ~5.4 [95% CI: 1.8, 8.7] and ~11.3 [95% CI:
7.9, 14.5] premature mortalities per 100,000 people, respectively (consistent with prior comparisons between these metrics;
330 Seltzer et al., 2018). Second, the diverging trends of the two exposure metrics (Fig. 3) are reflected in the estimated impacts (Fig.
7). Between 2000 and 2015, the MDA1 population-weighted exposure concentration decreased from ~53.7 ppb to ~48.3 ppb
(Table S2). As a result, the estimated human-health impacts using the J2009 parameters decreased from ~6.0 [95% CI: 2.0, 9.7]
to ~5.0 [95% CI: 1.7, 8.0] premature mortalities per 100,000 people (Table S5). In contrast, the MDA8 population-weighted
exposure concentration decreased from ~39.9 ppb to ~39.1 ppb, yet the impacts using the T2016 parameters increased from
335 ~10.8 [95% CI: 7.6, 13.8] to ~11.3 [95% CI: 7.9, 14.5] premature mortalities per 100,000 people (Fig. 7 and Table S5). These
differences in estimated impacts are not only due to changes in exposure. Over this period, an aging population structure
promoted increased susceptibility to O₃ impacts. In addition, depending on the age bin, baseline mortality rates for respiratory
diseases either marginally decreased or remained stable.

While exposure to long-term ambient O₃ for both metrics decreased between these end points, albeit by different magnitudes (-
340 25.5% vs. -5.7%), these other determinants played a strong role in modulating the trend in estimated impacts (Fig. 7). The net
change in 2015 vs. 2000 normalized human-health impacts using the J2009 and T2016 exposure-response relationships and
averaging metrics were -17.8% and +4.7%, respectively (black bars in Fig. 7). In both, an aging population structure



substantially eliminated much of the gains from exposure decreases (+15.5%). Changing baseline mortality rates were more modest, decreasing both calculations by -4.7%.

345 The differences in estimated human-health impacts when using the J2009 and T2016 exposure-response relationship and averaging metrics that are reported here are consistent with prior studies (Malley et al., 2017; Seltzer et al., 2018; Shindell et al., 2018). That is, the estimated human-health impacts when using the T2016 exposure-response relationship and averaging metric are considerably higher than the results computed when using the J2009 parameters. However, to our knowledge, the evolving differences between the two have yet to be shown. In 2000, the T2016 results were ~80% higher than the J2009 results (Table
350 S5). By 2008, the T2016 results were nearly double the J2009 results, and this difference continued to grow (~130% in 2015).

Between 2000-2015, our net estimated premature mortalities attributable to long-term O₃ exposure in the USA ranged from ~14,500-19,200 when using the J2009 parameters and ~29,800-37,600 when using the T2016 parameters. Largely, these results are lower than analogous prior studies that are based solely on CTM estimates of O₃ exposure. An exception is Zhang et al. (2018), who found comparable results when using the J2009 epidemiological study. However, Zhang et al., (2018) report a 13%
355 increase in premature mortalities attributable to long-term O₃ exposure in the United States between 1990-2010, despite O₃ decreases. We find a ~6.7% decrease in premature mortalities attributable to long-term O₃ exposure, albeit over 2000-2015. This is likely due to the dramatic decreases in O₃ precursor emissions that occurred post-2000 (Xing et al., 2012; Simon et al., 2015).

3.3.1 Crop-Loss

Agriculture impacts for each of the crop varieties considered here decreased from 2000-2015 (Fig. 8). When using the M12
360 metric, the estimated national RYL for maize and soybeans in 2000 were 4.6% and 16.3% (Fig. 8 and Table S5). These values decreased to 2.9% and 11.2% in 2015. When using the AOT40 metric, the estimated national RYL for maize, soybeans, and wheat for the year 2000 were 3.4%, 11.9%, and 12.1%, respectively. By 2015, these RYL values dropped to 1.6%, 4.8%, and 9.4%, respectively. Broadly, these estimated agriculture yield impacts are comparable to the global “ozone yield gaps” (i.e. RYL) modeled by Mills et al., (2018a), who considered the flux-based, stomatal uptake of O₃ for each crop.

365 Several other characteristics are consistent among all of the crop varieties and metric combinations considered here. For one, estimated RYL featured substantial inter-annual variability, indicating that the impacts calculated from a single year might not be representative of a particular period. For example, the RYL for soybeans, when using the AOT40 metric, increased from 7.8% in 2004 to 11.6% in 2005 - a nearly ~50% increase. Second, similar to Van Dingenen et al., (2009) and Lapina et al., (2016), impacts were consistently higher when utilizing the M12 metric and the associated concentration-response functions. These
370 differences also became amplified over time. The RYL for soybeans in 2000 using the M12 metric (16.3%) was ~37% higher than the RYL using the AOT40 metric (11.9%), but the difference increased to ~135% (11.2% vs. 4.8%) by 2015 (Table S5). These diverging trends occur for two reasons. First, the slopes of the two soybean concentration-response functions are different (Fig. S8). Second, the daytime O₃ concentrations approached the AOT40 threshold of 40 ppb post-2007 (Table S3). Since the AOT40 metric accumulates O₃ above 40 ppb, this drop below the threshold yielded disproportional improvements in AOT40
375 calculated RYL.

4 Uncertainties, Limitations, and Additional Remarks

Studies quantifying the health impacts attributable to long-term PM_{2.5} exposure oftentimes use higher-resolution products (i.e. 0.1° x 0.1°) that harness satellite data (e.g. Apte et al., 2015; Cohen et al., 2017; van Donkelaar et al., 2019). However, a number of complications prevent such products for surface O₃ (Duncan et al., 2014). Regardless, we believe this 0.5° x 0.5° product is of



380 sufficient resolution to estimate long-term O₃ exposure for a number of reasons. First, O₃ features a residence time on the order
of hours to days in the lower troposphere and in urban environments (Parrish et al., 2012; Monks et al., 2015), providing
sufficient time for localized mixing. Second, unlike short-term O₃ exposure, long-term O₃ exposure is less sensitive to singular
events that are more heterogeneous in space and time. Third, regional CTM studies report only marginal differences in O₃
concentrations and estimated impacts when scaling from 12 km to resolutions comparable to this analysis (Punger and West,
385 2013; Gan et al., 2016).

In terms of impacts, there is evidence that O₃ affects more than what was presented here. Several epidemiological studies suggest
that human-health impacts may extend to cardiovascular mortality (Jerrett et al., 2013; Crouse et al., 2015; Cakmak et al., 2016;
Turner et al., 2016; Lim et al., 2019). Separately, we also applied a log-linear exposure-response function when performing the
human-health calculations presented here since it is most common in the community. There is evidence that this relationship may
390 be linear (Di et al., 2017). For agriculture, the exposure-response functions utilized here are ‘pooled’ from studies featuring a
limited number of cultivars grown in the USA and Europe (Van Dingenen et al., 2009). While considered reliably representative
of the commonly grown cultivar population in these regions, extrapolation of these relationships to the national level may
introduce additional uncertainty. In addition, the methodology selected here does not take into account changes in plant
conditions that may limit or exacerbate conditions which influence the opening of stomata and the ability of a plant to uptake O₃,
395 such as temperature and soil moisture. Finally, it should be noted that O₃ exposure is associated with yield losses for several
other commercial and horticultural crops, including rice and cotton (Mills et al., 2007; Shindell et al., 2018).

Long-term trends of O₃ are driven by a number of mechanisms, including intercontinental transport (Fiore et al., 2009; Lin et al.,
2012; Lin et al., 2017) and methane concentrations (Fiore et al., 2002; Shindell et al., 2017; Lin et al., 2017). For example, Lin et
al., 2015 conclude that rising Asian emissions and global methane have played a key role in the increase of western USA
400 springtime O₃ from 1995-2014. These drivers merit additional exploration, on a seasonal basis and with the inclusion of
observations from the most recent years (i.e. 2015-2017). As Chinese emissions of NO_x peaked in 2012 (Zheng et al., 2018), our
current and future estimate of background O₃ trends and their influence on impact metrics might warrant revisiting.

The results presented here also demonstrate the need for additional epidemiological studies to test the utility of common
averaging metrics that are used when estimating health impacts. Specifically, clarity is needed regarding if long-term O₃ health-
405 impacts are more sensitive to peak averaged (i.e. the MDA1 metric) or annually averaged (i.e. the MDA8 metric) O₃
concentrations.

5 Conclusions

Through the application of artificial neural networks, we empirically model the magnitude, trends, and impacts of long-term (i.e.
months, annual) ambient O₃ over the continental United States from 2000-2015. We then used these estimates of long-term O₃
410 exposure to generate a measurement-based assessment of impacts on human-health and crop yields. All metrics with averaging
periods spanning the traditional ‘O₃ season’ featured peak exposure in 2002, with net decreases over the course of the study
period. For example, the population-weighted, April-September average of the daily 1-hour maximum O₃ concentration (i.e.
MDA1; from Jerrett et al., 2009) decreased by -0.43 [95% CI: -0.28, -0.57] ppb/yr between 2000-2015. In contrast, there was
little change in the population-weighted, annual average of the maximum daily 8-hour average O₃ concentration (i.e. MDA8;
415 from Turner et al., 2016) between 2000-2015. This was largely due to the compensating effects of wintertime O₃ increases and
summertime O₃ decreases; yielding a net population-weighted trend of -0.03 [95% CI: 0.04, -0.10] ppb/yr. Human-health metric
trends also featured an east-west divide, with stronger decreases in the eastern USA. All agriculture-weighted crop-loss metrics



featured decreasing trends over the study period.

Human-health impacts were quantified in terms of the estimated number of premature respiratory mortalities attributable to long-term O₃ exposure per 100,000 people. Crop-loss impacts were quantified in terms of the estimated national relative yield loss for a variety of commercial crops. Normalized human-health impacts estimates decreased by ~18% and increased by ~5% when using the Jerrett et al., 2009 and Turner et al., 2016 averaging metrics and parameters, respectively. In both cases, exposure changes and an aging population structure played a substantial role in modulating these trends. When using the M12 metric, the estimated national relative yield loss (RYL) for maize and soybeans between 2000 and 2015 decreased by 1.7% and 5.1%. When using the AOT40 metric, the net benefits over time were greater, with national reductions in RYL for maize, soybeans, and wheat decreasing by 1.9%, 7.1%, and 2.7%, respectively. These different responses are due to the daylight O₃ concentrations approaching the 40 ppb AOT40 threshold by the end of the study period and the differing slopes of the M12 vs. AOT40 concentration-response functions. Overall, these results provide a measurement-based estimate of long-term O₃ exposure over the United States, quantify the historical magnitude, trends, and impacts of such exposure, and illustrate how different conclusions regarding historical impacts can be made through the use of varying metrics.

Data Availability

Maps of the O₃ exposure metrics used in this study can be accessed by contacting one of the corresponding authors.

Author Contributions

All authors contributed to the design and/or methodology of the study. K.M.S. applied the methods, analyzed the results, developed all figures/tables, and drafted the initial manuscript. All authors edited and contributed to subsequent drafts of the manuscript.

Competing Interests

The authors declare that they have no conflicts of interest.

Acknowledgements

K.M.S. was supported by NASA Headquarters under the NASA Earth and Space Science Fellowship Program - Grant #80NSSC17K0354. All O₃ observations were retrieved from the TOAR database via the Representational State Transfer (REST) services. Special thanks to the TOAR team/community, particularly Owen Cooper, Martin Schultz, and Sabine Schröder, for compiling all of the observations into a variety of metrics, the MEIC team for providing Chinese anthropogenic emissions, and the Duke Compute Cluster for computational resources.

References

Abadi, M., Agarwal, A., Barham, P., Brevdo, E., Chen, Z., Citro, C., Corrado, G. S., Davis, A., Dean, J., Devin, M., Ghemawat, S., Goodfellow, I., Harp, A., Irving, G., Isard, M., Jia, Y., Jozefowicz, R., Kaiser, L., Kudlur, M., Levenberg, J., Mane, D., Monga, R., Moore, S., Murray, D., Olah, C., Schuster, M., Shlens, J., Steiner, B., Sutskever, I., Talwar, K., Tucker, P.,



- Vanhoucke, V., Vasudevan, V., Viegas, F., Vinyals, O., Warden, P., Wattenberg, M., Wicke, M., Yu, Y. and Zheng, X.: TensorFlow: Large-Scale Machine Learning on Heterogeneous Distributed Systems, Available from: <http://arxiv.org/abs/1603.04467>, 2016.
- 450 Anenberg, S. C., Horowitz, L. W., Tong, D. Q. and West, J. J.: An estimate of the global burden of anthropogenic ozone and fine particulate matter on premature human mortality using atmospheric modeling, *Environ. Health Perspect.*, 118(9), 1189–1195, doi:10.1289/ehp.0901220, 2010.
- 455 Apte, J. S., Marshall, J. D., Cohen, A. J. and Brauer, M.: Addressing Global Mortality from Ambient PM_{2.5}, *Environ. Sci. Technol.*, 49, 8057–8066, doi:10.1021/acs.est.5b01236, 2015.
- Avnery, S., Mauzerall, D. L., Liu, J. and Horowitz, L. W.: Global crop yield reductions due to surface ozone exposure: 1. Year 2000 crop production losses and economic damage, *Atmos. Environ.*, 45, 2284–2296, doi:10.1016/j.atmosenv.2010.11.045, 2011.
- 460 Bell, M. L.: The use of ambient air quality modeling to estimate individual and population exposure for human health research: A case study of ozone in the Northern Georgia Region of the United States, *Environ. Int.*, 32, 586–593, doi:10.1016/j.envint.2006.01.005, 2006.
- Berrocal, V. J., Gelfand, A. E. and Holland, D. M.: Space-Time Data fusion Under Error in Computer Model Output: An Application to Modeling Air Quality, *Biometrics*, 68(3), 837–848, doi:10.1111/j.1541-0420.2011.01725.x, 2012.
- 465 Bey, I., Jacob, D. J., Yantosca, R. M., Logan, J. A., Field, B. D., Fiore, A. M., Li, Q., Liu, H. Y., Mickley, L. J. and Schultz, M. G.: Global modeling of tropospheric chemistry with assimilated meteorology: Model description and evaluation, *J. Geophys. Res.*, 106(D19), 23073–23095, doi:10.1029/2001jd000807, 2001.
- Bloomer, B. J., Vinnikov, K. Y. and Dickerson, R. R.: Changes in seasonal and diurnal cycles of ozone and temperature in the eastern U.S., *Atmos. Environ.*, 44(21–22), 2543–2551, doi:10.1016/j.atmosenv.2010.04.031, 2010.
- 470 Brauer, M., Lencar, C., Tamburic, L., Koehoorn, M., Demers, P. and Karr, C.: A Cohort Study of Traffic-Related Air Pollution Impacts on Birth Outcomes, *Environ. Health Perspect.*, 116(5), 680–686, doi:10.1289/ehp.10952, 2008.
- Cakmak, S., Hebber, C., Vanos, J., Crouse, D. L. and Burnett, R.: Ozone exposure and cardiovascular-related mortality in the Canadian Census Health and Environment Cohort (CANCHEC) by spatial synoptic classification zone, *Environ. Pollut.*, 214(2), 589–599, doi:10.1016/j.envpol.2016.04.067, 2016.
- 475 Camalier, L., Cox, W. and Dolwick, P.: The effects of meteorology on ozone in urban areas and their use in assessing ozone trends, *Atmos. Environ.*, 41(33), 7127–7137, doi:10.1016/j.atmosenv.2007.04.061, 2007.
- Chameides, W. L., Kasibhatla, P. S., Yienger, J. and Levy II, H.: Growth of Continental-Scale Metro-Agro-Plexes, Regional Ozone Pollution, and World Food Production, *Science*, 264(5155), 74–77, 1994.
- Chang, H. H., Zhou, J. and Fuentes, M.: Impact of climate change on ambient ozone level and mortality in Southeastern United States, *Int. J. Environ. Res. Public Health*, 7(7), 2866–2880, doi:10.3390/ijerph7072866, 2010.
- 480 Chang, K.-L., Petropavlovskikh, I., Copper, O. R., Schultz, M. G. and Wang, T.: Regional trend analysis of surface ozone observations from monitoring networks in eastern North America, Europe and East Asia, *Elem. Sci. Anthr.*, 5(50), doi:10.1525/elementa.243, 2017.
- Chollet, F. keras, GitHub. <https://github.com/fchollet/keras>, 2015.
- 485 Center for International Earth Science Information Network - CIESIN - Columbia University. Gridded Population of the World, Version 4 (GPWv4): Population Density Adjusted to Match 2015 Revision UN WPP Country Totals. Palisades, NY: NASA Socioeconomic Data and Applications Center (SEDAC); doi: 10.7927/H4HX19NJ, 2016.
- Clifton, O. E., Fiore, A. M., Correa, G., Horowitz, L. W. and Naik, V.: Twenty-first century reversal of the surface ozone



- seasonal cycle over the northeastern United States, *Geophys. Res. Lett.*, 41, 7343–7350, doi:10.1002/2014GL061378, 2014.
- 490 Cohen, A. J., Brauer, M., Burnett, R., Anderson, H. R., Frostad, J., Estep, K., Balakrishnan, K., Brunekreef, B., Dandona, L.,
Dandona, R., Feigin, V., Freedman, G., Hubbell, B., Jobling, A., Kan, H., Knibbs, L., Liu, Y., Martin, R., Morawska, L., Pope,
C. A., Shin, H., Straif, K., Shadick, G., Thomas, M., van Dingenen, R., van Donkelaar, A., Vos, T., Murray, C. J. L. and
Forouzanfar, M. H.: Estimates and 25-year trends of the global burden of disease attributable to ambient air pollution: an analysis
of data from the Global Burden of Diseases Study 2015, *Lancet*, 389(10082), 1907–1918, doi:10.1016/S0140-6736(17)30505-6,
495 2017.
- Comrie, A. C.: Comparing Neural Networks and Regression Models for Ozone Forecasting, *J. Air Waste Manag. Assoc.*, 47(6),
653–663, doi:10.1080/10473289.1997.10463925, 1997.
- Cooper, O. R., Gao, R. S., Tarasick, D., Leblanc, T. and Sweeney, C.: Long-term ozone trends at rural ozone monitoring sites
across the United States, 1990–2010, *J. Geophys. Res. Atmos.*, 117(22), 1990–2010, doi:10.1029/2012JD018261, 2012.
- 500 Cooper, O. R., Parrish, D. D., Ziemke, J., Balashov, N. V., Cupeiro, M., Galbally, I. E., Gilge, S., Horowitz, L., Jensen, N. R.,
Lamarque, J.-F., Naik, V., Oltmans, S. J., Schwab, J., Shindell, D. T., Thompson, A. M., Thourret, V., Wang, Y. and Zbinden, R.
M.: Global distribution and trends of tropospheric ozone: An observation-based review, *Elem. Sci. Anthr.*, 2,
doi:10.12952/journal.elementa.000029, 2014.
- Crouse, D. L., Peters, P. A., Hystad, P., Brook, J. R., van Donkelaar, A., Martin, R. V., Villeneuve, P. J., Jerrett, M., Goldberg,
505 M. S., Arden Pope, C., Brauer, M., Brook, R. D., Robichaud, A., Menard, R. and Burnett, R. T.: Ambient PM_{2.5}, O₃, and NO₂
exposures and associations with mortality over 16 years of follow-up in the canadian census health and environment cohort
(CanCHEC), *Environ. Health Perspect.*, 123(11), 1180–1186, doi:10.1289/ehp.1409276, 2015.
- Di, Q., Rowland, S., Koutrakis, P. and Schwartz, J.: A hybrid model for spatially and temporally resolved ozone exposures in the
continental United States, *J. Air Waste Manag. Assoc.*, 67(1), 39–52, doi:10.1080/10962247.2016.1200159, 2017.
- 510 Doherty, R. M., Wild, O., Shindell, D. T., Zeng, G., MacKenzie, I. A., Collins, W. J., Fiore, A. M., Stevenson, D. S., Dentener,
F. J., Schultz, M. G., Hess, P., Derwent, R. G. and Keating, T. J.: Impacts of climate change on surface ozone and
intercontinental ozone pollution: A multi-model study, *J. Geophys. Res. Atmos.*, 118(9), 3744–3763,
doi:10.1002/jgrd.502662013, 2013.
- Duncan, B. N., Prados, A. I., Lamsal, L. N., Liu, Y., Streets, D. G., Gupta, P., Hilsenrath, E., Kahn, R. A., Nielsen, J. E.,
515 Beyersdorf, A. J., Burton, S. P., Fiore, A. M., Fishman, J., Henze, D. K., Hostetler, C. A., Krotkov, N. A., Lee, P., Lin, M.,
Pawson, S., Pfister, G., Pickering, K. E., Pierce, R. B., Yoshida, Y. and Ziemba, L. D.: Satellite data of atmospheric pollution for
U.S. air quality applications: Examples of applications, summary of data end-user resources, answers to FAQs, and common
mistakes to avoid, *Atmos. Environ.*, 94, 647–662, doi:10.1016/j.atmosenv.2014.05.061, 2014.
- Dutot, A. L., Rynkiewicz, J., Steiner, F. E. and Rude, J.: A 24-h forecast of ozone peaks and exceedance levels using neural
520 classifiers and weather predictions, *Environ. Model. Softw.*, 22, 1261–1269, doi:10.1016/j.envsoft.2006.08.002, 2007.
- Fairlie, T. D., Jacob, D. J. and Park, R. J.: The impact of transpacific transport of mineral dust in the United States, *Atmos.
Environ.*, 41, 1251–1266, doi:10.1016/j.atmosenv.2006.09.048, 2007.
- FAO. FAOSTAT: United Nations Food and Agriculture Organization statistical databases. Retrieved from [http://faostat.fao.org/
site/339/default.aspx](http://faostat.fao.org/site/339/default.aspx), 2010.
- 525 Fiore, A. M., Jacob, D. J., Field, B. D., Streets, D. G., Fernandes, S. D. and Jang, C.: Linking ozone pollution and climate
change: The case for controlling methane, *Geophys. Res. Lett.*, 29(19), doi:10.1029/2002gl015601, 2002.
- Fiore, A. M., Dentener, F. J., Wild, O., Cuvelier, C., Schultz, M. G., Hess, P., Textor, C., Schulz, M., Doherty, R. M., Horowitz,
L. W., MacKenzie, I. A., Sanderson, M. G., Shindell, D. T., Stevenson, D. S., Szopa, S., Van Dingenen, R., Zeng, G., Atherton,



- C., Bergmann, D., Bey, I., Carmichael, G., Collins, W. J., Duncan, B. N., Faluvegi, G., Folberth, G., Gauss, M., Gong, S.,
530 Hauglustaine, D., Holloway, T., Isaksen, I. S. A., Jacob, D. J., Jonson, J. E., Kaminski, J. W., Keating, T. J., Lupu, A., Marmer,
E., Montanaro, V., Park, R. J., Pitari, G., Pringle, K. J., Pyle, J. A., Schroeder, S., Vivanco, M. G., Wind, P., Wojcik, G., Wu, S.
and Zuber, A.: Multimodel estimates of intercontinental source-receptor relationships for ozone pollution, *J. Geophys. Res.*,
114(D04301), doi:10.1029/2008JD010816, 2009.
- Fix, M. J., Cooley, D., Hodzic, A., Gilleland, E., Russell, B. T., Porter, W. C. and Pfister, G. G.: Observed and predicted
535 sensitivities of extreme surface ozone to meteorological drivers in three US cities, *Atmos. Environ.*, 176(December 2017), 292–
300, doi:10.1016/j.atmosenv.2017.12.036, 2018.
- Fleming, Z. L., Doherty, R. M., Von Schneidemesser, E., Malley, C. S., Cooper, O. R., Pinto, J. P., Colette, A., Xu, X., Simpson,
D., Schultz, M. G., Lefohn, A. S., Hamad, S., Moolla, R., Solberg, S. and Feng, Z.: Tropospheric Ozone Assessment Report:
Present-day ozone distribution and trends relevant to human health, *Elem. Sci. Anthr.*, 6(12), doi:10.1525/elementa.273, 2018.
- 540 Fountoukis, C. and Nenes, A.: ISORROPIA II: a computationally efficient thermodynamic equilibrium model for K^+ – Ca^{2+} –
 Mg^{2+} – NH_4^+ – Na^+ – SO_4^{2-} – NO_3^- – Cl^- – H_2O aerosols, *Atmos. Chem. Phys.*, 7, 4639–4659, doi:10.5194/acp-7-4639-2007,
2007.
- Gan, C., Hogrefe, C., Mathur, R., Pleim, J., Xing, J., Wong, D., Gilliam, R., Pouliot, G. and Wei, C.: Assessment of the effects of
horizontal grid resolution on long-term air quality trends using coupled WRF-CMAQ simulations, *Atmos. Environ.*, 132, 207–
545 216, doi:10.1016/j.atmosenv.2016.02.036, 2016.
- Gardner, M. W. and Dorling, S. R.: Statistical surface ozone models: An improved methodology to account for non-linear
behaviour, *Atmos. Environ.*, 34, 21–34, doi:10.1016/S1352-2310(99)00359-3, 2000.
- Gaudel, A., Cooper, O. R., Ancellet, G., Barret, B., Boynard, A., Burrows, J. P., Clerbaux, C., Coheur, P.-F., Cuesta, J., Cuevas,
E., Doniki, S., Dufour, G., Ebojic, F., Foret, G., Garcia, O., Granados Muñoz, M. J., Hannigan, J. W., Hase, F., Hassler, B.,
550 Huang, G., Hurtmans, D., Jaffé, D., Jones, N., Kalabokas, P., Kerridge, B., Kulawik, S. S., Latter, B., Leblanc, T., Le
Flochmoën, E., Lin, W., Liu, J., Liu, X., Mahieu, E., McClure-Begley, A., Neu, J. L., Osman, M., Palm, M., Petetin, H.,
Petropavlovskikh, I., Querel, R., Rapp, N., Rozanov, A., Schultz, M. G., Schwab, J., Siddans, R., Smale, D., Steinbacher, M.,
Tanimoto, H., Tarasick, D. W., Thouret, V., Thompson, A. M., Trickl, T., Weatherhead, E., Wespes, C., Worden, H. M.,
Vigouroux, C., Xu, X., Zeng, G. and Ziemke, J.: Tropospheric Ozone Assessment Report: Present-day distribution and trends of
555 tropospheric ozone relevant to climate and global atmospheric chemistry model evaluation, *Elem. Sci. Anthr.*, 6(39),
doi:10.1525/elementa.291, 2018.
- Guo, J. J., Fiore, A. M., Murray, L. T., Jaffé, D. A., Schnell, J. L., Moore, C. T. and Milly, G. P.: Average versus high surface
ozone levels over the continental USA: Model bias, background influences, and interannual variability, *Atmos. Chem. Phys.*, 18,
12123–12140, doi:10.5194/acp-18-12123-2018, 2018.
- 560 Hoesly, R. M., Smith, S. J., Feng, L., Klimont, Z., Janssens-maenhout, G., Pitkanen, T., Seibert, J., Vu, L., Andres, R., Bolt, R.,
Bond, T., Dawidowski, L., Kholod, N., Kurokawa, J., Li, M., Liu, L., Lu, Z., Moura, M. C., O'Rourke, P. and Zhang, Q.:
Historical (1750 – 2014) anthropogenic emissions of reactive gases and aerosols from the Community Emissions Data System
(CEDS), *Geosci. Model Dev.*, 11, 369–408, doi:10.5194/gmd-11-369-2018, 2018.
- Hu, L., Keller, C. A., Long, M. S., Sherwen, T., Auer, B., Da Silva, A., Nielsen, J. E., Pawson, S., Thompson, M. A., Trayanov,
565 A. L., Travis, K. R., Grange, S. K., Evans, M. J. and Jacob, D. J.: Global simulation of tropospheric chemistry at 12.5 km
resolution: performance and evaluation of the GEOS-Chem chemical module (v10-1) within the NASA GEOS Earth system
model (GEOS-5 ESM), *Geosci. Model Dev.*, 11, 4603–4620, doi:10.5194/gmd-11-4603-2018, 2018.
- Jacob, D. J. and Winner, D. A.: Effect of climate change on air quality, *Atmos. Environ.*, 43(1), 51–63,



doi:10.1016/j.atmosenv.2008.09.051, 2009.

- 570 Jaeglé, L., Quinn, P. K., Bates, T. S., Alexander, B. and Lin, J. T.: Global distribution of sea salt aerosols: New constraints from in situ and remote sensing observations, *Atmos. Chem. Phys.*, 11, 3137–3157, doi:10.5194/acp-11-3137-2011, 2011.
- Jaffe, D. and Ray, J.: Increase in surface ozone at rural sites in the western US, *Atmos. Environ.*, 41(26), 5452–5463, doi:10.1016/j.atmosenv.2007.02.034, 2007.
- Jaffe, D. A., Cooper, O. R., Fiore, A. M., Henderson, B. H., Tonneson, G. S., Russell, A. G., Henze, D. K., Langford, A. O., Lin, M. and Moore, T.: Scientific assessment of background ozone over the U.S.: Implications for air quality management, *Elem. Sci. Anthr.*, 6(56), doi:10.1525/elementa.309, 2018.
- Jerrett, M., Burnett, R. T., Pope, C. A., Ito, K., Thurston, G., Krewski, D., Shi, Y., Calle, E. and Thun, M.: Long-Term Ozone Exposure and Mortality, *N. Engl. J. Med.*, 360(11), 1085–1095, doi:10.1056/nejmoa0803894, 2009.
- Jerrett, M., Burnett, R. T., Beckerman, B. S., Turner, M. C., Krewski, D., Thurston, G., Martin, R. V., van Donkelaar, A., 580 Hughes, E., Shi, Y., Gapstur, S. M., Thun, M. J. and Pope, C. A.: Spatial Analysis of Air Pollution and Mortality in California, *Am. J. Respir. Crit. Care Med.*, 188(5), 593–599, doi:10.1164/rccm.201303-0609oc, 2013.
- Keller, C. A., Long, M. S., Yantosca, R. M., Da Silva, A. M., Pawson, S. and Jacob, D. J.: HEMCO v1.0: A versatile, ESMF-compliant component for calculating emissions in atmospheric models, *Geosci. Model Dev.*, 7, 1409–1417, doi:10.5194/gmd-7-1409-2014, 2014.
- 585 Kingma, D. P. and Ba, J.: Adam: A Method for Stochastic Optimization, *Conf. Pap. 3rd Int. Conf. Learn. Represent. San Diego, CA*. Available from: <http://arxiv.org/abs/1412.6980>, 2015.
- Lapina, K., Henze, D. K., Milford, J. B. and Travis, K.: Impacts of Foreign, Domestic, and State-Level Emissions on Ozone-Induced Vegetation Loss in the United States, *Environ. Sci. Technol.*, 50(2), 806–813, doi:10.1021/acs.est.5b04887, 2016.
- Lefohn, A. S., Malley, C. S., Simon, H., Wells, B., Xu, X., Zhang, L. and Wang, T.: Responses of human health and vegetation 590 exposure metrics to changes in ozone concentration distributions in the European Union, United States, and China, *Atmos. Environ.*, 152, 123–145, doi:10.1016/j.atmosenv.2016.12.025, 2017.
- Lefohn, A. S., Malley, C. S., Smith, L., Wells, B., Hazucha, M., Simon, H., Naik, V., Mills, G., Schultz, M. G., Paoletti, E., De Marco, A., Xu, X., Zhang, L., Wang, T., Neufeld, H. S., Musselman, R. C., Tarasick, D., Brauer, M., Feng, Z., Tang, H., Kobayashi, K., Sicard, P., Solberg, S. and Gerosa, G.: Tropospheric ozone assessment report: Global ozone metrics for climate 595 change, human health, and crop/ecosystem research, *Elem. Sci. Anthr.*, 6(28), doi:10.1525/elementa.279, 2018.
- Lelieveld, J., Barlas, C., Giannadaki, D. and Pozzer, A.: Model calculated global, regional and megacity premature mortality due to air pollution, *Atmos. Chem. Phys.*, 13(14), 7023–7037, doi:10.5194/acp-13-7023-2013, 2013.
- Lelieveld, J., Evans, J. S., Fnais, M., Giannadaki, D. and Pozzer, A.: The contribution of outdoor air pollution sources to premature mortality on a global scale, *Nature*, 525, 367–371, doi:10.1038/nature15371, 2015.
- 600 Li, K., Jacob, D. J., Liao, H., Shen, L., Zhang, Q. and Bates, K. H.: Anthropogenic drivers of 2013–2017 trends in summer surface ozone in China, *Proc. Natl. Acad. Sci.*, 116(2), 422–427, doi:10.1073/pnas.1812168116, 2019.
- Liang, C. K., West, J. J., Silva, R. A., Bian, H., Chin, M., Davila, Y., Dentener, F. J., Emmons, L., Flemming, J., Folberth, G., Henze, D., Im, U., Jonson, J. E., Keating, T. J., Kuesera, T., Lenzen, A., Lin, M., Tronstad Lund, M., Pan, X., Park, R. J., Pierce, R. B., Sekiya, T., Sudo, K. and Takemura, T.: HTAP2 multi-model estimates of premature human mortality due to 605 intercontinental transport of air pollution and emission sectors, *Atmos. Chem. Phys.*, 18(14), 10497–10520, doi:10.5194/acp-18-10497-2018, 2018.
- Lim, C. C., Hayes, R. B., Ahn, J., Shao, Y., Silverman, D. T., Jones, R. R., Garcia, C., Bell, M. L. and Thurston, G. D.: Long-term Exposure to Ozone and Cause-Specific Mortality Risk in the U.S., *Am. J. Respir. Crit. Care Med.*,



- doi:10.1164/rccm.201806-1161OC, 2019.
- 610 Lin, C. Y. C., Jacob, D. J. and Fiore, A. M.: Trends in exceedances of the ozone air quality standard in the continental United States, 1980-1998, *Atmos. Environ.*, 35(19), 3217–3228, doi:10.1016/S1352-2310(01)00152-2, 2001.
- Lin, M., Fiore, A. M., Horowitz, L. W., Cooper, O. R., Naik, V., Holloway, J., Johnson, B. J., Middlebrook, A. M., Oltmans, S. J., Pollack, I. B., Ryerson, T. B., Warner, J. X., Wiedinmyer, C., Wilson, J. and Wyman, B.: Transport of Asian ozone pollution into surface air over the western United States in spring, *J. Geophys. Res.*, 117(D00V07), doi:10.1029/2011JD016961, 2012.
- 615 Lin, M., Horowitz, L. W., Cooper, O. R., Tarasick, D., Conley, S., Iraci, L. T., Johnson, B., Leblanc, T., Petropavlovskikh, I. and Yates, E. L.: Revisiting the evidence of increasing springtime ozone mixing ratios in the free troposphere over western North America, *Geophys. Res. Lett.*, 42, 8719–8728, doi:10.1002/2015GL065311, 2015.
- Lin, M., Horowitz, L. W., Payton, R., Fiore, A. M. and Tonnesen, G.: US surface ozone trends and extremes from 1980 to 2014: Quantifying the roles of rising Asian emissions, domestic controls, wildfires, and climate, *Atmos. Chem. Phys.*, 17, 2943–2970, doi:10.5194/acp-17-2943-2017, 2017.
- 620 Malley, C. S., Henze, D. K., Kuylenstierna, J. C. I., Vallack, H. W., Davila, Y., Anenberg, S. C., Turner, M. C. and Ashmore, M. R.: Updated Global Estimates of Respiratory Mortality in Adults ≥ 30 Years of Age Attributable to Long-Term Ozone Exposure, *Environ. Health Perspect.*, 125, doi:10.1289/ehp1390, 2017.
- Marshall, J. D., Nethery, E. and Brauer, M.: Within-urban variability in ambient air pollution: Comparison of estimation methods, *Atmos. Environ.*, 42, 1359–1369, doi:10.1016/j.atmosenv.2007.08.012, 2008.
- Mauzerall, D. L. and Wang, X.: Protecting Agricultural Crops from the Effects of Tropospheric Ozone Exposure: Reconciling Science and Standard Setting in the United States, Europe, and Asia, *Annu. Rev. Energy Environ.*, 26, 237–268, doi:10.1146/annurev.energy.26.1.237, 2001.
- 630 Mills, G., Buse, A., Gimeno, B., Bermejo, V., Holland, M., Emberson, L. and Pleijel, H.: A synthesis of AOT40-based response functions and critical levels of ozone for agricultural and horticultural crops, *Atmos. Environ.*, 41, 2630–2643, doi:10.1016/j.atmosenv.2006.11.016, 2007.
- Mills, G., Sharps, K., Simpson, D., Pleijel, H., Frei, M., Burkey, K., Emberson, L., Uddling, J., Broberg, M., Feng, Z., Kobayashi, K. and Agrawal, M.: Closing the global ozone yield gap: Quantification and cobenefits for multistress tolerance, *Glob. Chang. Biol.*, (June), 4869–4893, doi:10.1111/gcb.14381, 2018a.
- 635 Mills, G., Pleijel, H., Malley, C. S., Sinha, B., Cooper, O. R., Schultz, M. G., Neufeld, H. S., Simpson, D., Sharps, K., Feng, Z., Gerosa, G., Harmens, H., Kobayashi, K., Saxena, P., Paoletti, E., Sinha, V. and Xu, X.: Tropospheric Ozone Assessment Report: Present-day tropospheric ozone distribution and trends relevant to vegetation, *Elem. Sci. Anthr.*, 6(47), doi:10.1525/elementa.302, 2018b.
- Monks, P. S., Archibald, A. T., Colette, A., Cooper, O., Coyle, M., Derwent, R., Fowler, D., Granier, C., Law, K. S., Mills, G. E., Stevenson, D. S., Tarasova, O., Thouret, V., Von Schneidmesser, E., Sommariva, R., Wild, O. and Williams, M. L.: Tropospheric ozone and its precursors from the urban to the global scale from air quality to short-lived climate forcer, *Atmos. Chem. Phys.*, 15, 8889–8973, doi:10.5194/acp-15-8889-2015, 2015.
- 640 Park, R. J., Jacob, D. J., Chin, M. and Martin, R. V.: Sources of carbonaceous aerosols over the United States and implications for natural visibility, *J. Geophys. Res.*, 108(D12), doi:10.1029/2002JD003190, 2003.
- 645 Park, R. J., Jacob, D. J., Field, B. D., Yantosca, R. M. and Chin, M.: Natural and transboundary pollution influences on sulfate-nitrate-ammonium aerosols in the United States: Implications for policy, *J. Geophys. Res.*, 109(D15204), doi:10.1029/2003JD004473, 2004.
- Parrish, D. D., Law, K. S., Staehelin, J., Derwent, R., Cooper, O. R., Tanimoto, H., Volz-Thomas, A., Gilge, S., Scheel, H.-E.,



- Steinbacher, M. and Chan, E.: Long-term changes in lower tropospheric baseline ozone concentrations at northern mid-latitudes, *Atmos. Chem. Phys.*, 12(23), 11485–11504, doi:10.5194/acp-12-11485-2012, 2012.
- Porter, W. C., Heald, C. L., Cooley, D. and Russell, B.: Investigating the observed sensitivities of air-quality extremes to meteorological drivers via quantile regression, *Atmos. Chem. Phys.*, 15(18), 10349–10366, doi:10.5194/acp-15-10349-2015, 2015.
- Porter, W. C., Safieddine, S. A. and Heald, C. L.: Impact of aromatics and monoterpenes on simulated tropospheric ozone and total OH reactivity, *Atmos. Environ.*, 169, 250–257, doi:10.1016/j.atmosenv.2017.08.048, 2017.
- Punger, E. M. and West, J. J.: The effect of grid resolution on estimates of the burden of ozone and fine particulate matter on premature mortality in the USA, *Air Qual. Atmos. Heal.*, 6(3), 563–573, doi:10.1007/s11869-013-0197-8, 2013.
- Pye, H. O. T., Liao, H., Wu, S., Mickley, L. J., Jacob, D. J., Henze, D. J. and Seinfeld, J. H.: Effect of changes in climate and emissions on future sulfate-nitrate-ammonium aerosol levels in the United States, *J. Geophys. Res. Atmos.*, 114(1), 1–18, doi:10.1029/2008JD010701, 2009.
- Ruiz-Suárez, J. C., Mayora-Ibarra, O. A., Torres-Jiménez, J. and Ruiz-Suárez, L. G.: Short-term ozone forecasting by artificial neural networks, *Adv. Eng. Softw.*, 23, 143–149, doi:10.1016/0965-9978(95)00076-3, 1995.
- Russell, B. T., Cooley, D. S., Porter, W. C. and Heald, C. L.: Modeling the spatial behavior of the meteorological drivers' effects on extreme ozone, *Environmetrics*, 27(6), 334–344, doi:10.1002/env.2406, 2016.
- Schnell, J. L., Prather, M. J., Josse, B., Naik, V., Horowitz, L. W., Cameron-Smith, P., Bergmann, D., Zeng, G., Plummer, D. A., Sudo, K., Nagashima, T., Shindell, D. T., Faluvegi, G. and Strode, S. A.: Use of North American and European air quality networks to evaluate global chemistry–climate modeling of surface ozone, *Atmos. Chem. Phys.*, 15, 10581–10596, doi:10.5194/acp-15-10581-2015, 2015.
- Schultz, M. G., Schröder, S., Lyapina, O., Cooper, O., Galbally, I., Petropavlovskikh, I., Von Schneidmesser, E., Tanimoto, H., Elshorbany, Y., Naja, M., Seguel, R., Dauert, U., Eckhardt, P., Feigenspahn, S., Fiebig, M., Hjellbrekke, A.-G., Hong, Y.-D., Christian Kjeld, P., Koide, H., Lear, G., Tarasick, D., Ueno, M., Wallasch, M., Baumgardner, D., Chuang, M.-T., Gillett, R., Lee, M., Molloy, S., Moolla, R., Wang, T., Sharps, K., Adame, J. A., Ancellet, G., Apadula, F., Artaxo, P., Barlasina, M., Bogucka, M., Bonasoni, P., Chang, L., Colomb, A., Cuevas-Agullo, E., Cupeiro, M., Degorska, A., Ding, A., Fröhlich, M., Frolova, M., Gadhavi, H., Gheusi, F., Gilge, S., Gonzalez, M. Y., Gros, V., Hamad, S. H., Helmig, D., Henriques, D., Hermansen, O., Holla, R., Huber, J., Im, U., Jaffe, D. A., Komala, N., Kubistin, D., Lam, K.-S., Laurila, T., Lee, H., Levy, I., Mazzoleni, C., Mazzoleni, L., McClure-Begley, A., Mohamad, M., Murovic, M., Navarro-Comas, M., Nicodim, F., Parrish, D., Read, K. A., Reid, N., Ries, L., Saxena, P., Schwab, J. J., Scorgie, Y., Senik, I., Simmonds, P., Sinha, V., Skorokhod, A., Spain, G., Spangl, W., Spoor, R., Springston, S. R., Steer, K., Steinbacher, M., Suharguniyawan, E., Torre, P., Trickl, T., Weili, L., Weller, R., Xu, X., Xue, L. and Zhiqiang, M.: Tropospheric Ozone Assessment Report: Database and Metrics Data of Global Surface Ozone Observations, *Elem. Sci. Anthr.*, 5(58), doi:10.1525/elementa.244, 2017.
- Seltzer, K. M., Shindell, D. T., Faluvegi, G. and Murray, L. T.: Evaluating Modeled Impact Metrics for Human Health, Agriculture Growth, and Near-Term Climate, *J. Geophys. Res. Atmos.*, 122, 13,506–13,524, doi:10.1002/2017JD026780, 2017.
- Seltzer, K. M., Shindell, D. T. and Malley, C. S.: Measurement-based assessment of health burdens from long-term ozone exposure in the United States, Europe, and China, *Environ. Res. Lett.*, 13, doi:10.1088/1748-9326/aae29d, 2018.
- Shindell, D., Faluvegi, G., Seltzer, K. and Shindell, C.: Quantified, localized health benefits of accelerated carbon dioxide emissions reductions, *Nat. Clim. Chang.*, 8, 1–5, doi:10.1038/s41558-018-0108-y, 2018.
- Shindell, D., Faluvegi, G., Kasibhatla, P. and Van Dingenen, R.: Spatial Patterns of Crop Yield Change by Emitted Pollutant, *Earth's Futur.*, 7, 101–112, doi:10.1029/2018EF001030, 2019.



- Shindell, D. T., Pechony, O., Voulgarakis, A., Faluvegi, G., Nazarenko, L., Lamarque, J. F., Bowman, K., Milly, G., Kovari, B.,
690 Ruedy, R. and Schmidt, G. A.: Interactive ozone and methane chemistry in GISS-E2 historical and future climate simulations,
Atmos. Chem. Phys., 13(5), 2653–2689, doi:10.5194/acp-13-2653-2013, 2013.
- Shindell, D. T., Fuglestedt, J. S. and Collins, W. J.: The social cost of methane: theory and applications, *Faraday Discuss.*, 200,
429–451, doi:10.1039/c7fd00009j, 2017.
- Silva, R. A., West, J. J., Zhang, Y., Anenberg, S. C., Lamarque, J. F., Shindell, D. T., Collins, W. J., Dalsoren, S., Faluvegi, G.,
695 Folberth, G., Horowitz, L. W., Nagashima, T., Naik, V., Rumbold, S., Skeie, R., Sudo, K., Takemura, T., Bergmann, D.,
Cameron-Smith, P., Cionni, I., Doherty, R. M., Eyring, V., Josse, B., Mackenzie, I. A., Plummer, D., Righi, M., Stevenson, D.
S., Strode, S., Szopa, S. and Zeng, G.: Global premature mortality due to anthropogenic outdoor air pollution and the
contribution of past climate change, *Environ. Res. Lett.*, 8, doi:10.1088/1748-9326/8/3/034005, 2013.
- Simon, H., Reff, A., Wells, B., Xing, J. and Frank, N.: Ozone trends across the United States over a period of decreasing NO_x
700 and VOC emissions, *Environ. Sci. Technol.*, 49, 186–195, doi:10.1021/es504514z, 2015.
- Stanaway, J. D., Afshin, A., Gakidou, E., Lim, S. S., Abate, D., Abate, K. H., Abbafati, C., Abbasi, N., Abbastabar, H., Abd-
Allah, F., Abdela, J., Abdelalim, A., Abdollahpour, I., Abdulkader, R. S., Abebe, M., Abebe, Z., Abera, S. F., Abil, O. Z.,
Abraha, H. N., Abrham, A. R., Abu-Raddad, L. J., Abu-Rmeileh, N. M. E., Accrombessi, M. M. K., Acharya, D., Acharya, P.,
Adamu, A. A., Adane, A. A., Adebayo, O. M., Adedoyin, R. A., Adekanmbi, V., Ademi, Z., Adetokunboh, O. O., Adib, M. G.,
705 Admasie, A., Adsuar, J. C., Afanvi, K. A., Afarideh, M., Agarwal, G., Aggarwal, A., Aghayan, S. A., Agrawal, A., Agrawal, S.,
Ahmadi, A., Ahmadi, M., Ahmadi, H., Ahmed, M. B., Aichour, A. N., Aichour, I., Aichour, M. T. E., Akbari, M. E.,
Akinyemiju, T., Akseer, N., Al-Aly, Z., Al-Eyadhy, A., Al-Mekhlafi, H. M., Alahdab, F., Alam, K., Alam, S., Alam, T., Alashi,
A., Alavian, S. M., Alene, K. A., Ali, K., Ali, S. M., Alijanzadeh, M., Alizadeh-Navaei, R., Aljunid, S. M., Alkerwi, A., Alla, F.,
Alsharif, U., Altirkawi, K., Alvis-Guzman, N., Amare, A. T., Ammar, W., Anber, N. H., Anderson, J. A., Andrei, C. L.,
710 Androudi, S., Animut, M. D., Anjomshoa, M., Ansha, M. G., Antó, J. M., Antonio, C. A. T., Anwari, P., Appiah, L. T., Appiah,
S. C. Y., Arabloo, J., Aremu, O., Ärnlov, J., Artaman, A., Aryal, K. K., Asayesh, H., Ataro, Z., Ausloos, M., Avokpaho, E. F. G.
A., Awasthi, A., Quintanilla, B. P. A., Ayer, R., Ayuk, T. B., et al.: Global, regional, and national comparative risk assessment of
84 behavioural, environmental and occupational, and metabolic risks or clusters of risks for 195 countries and territories, 1990-
2017: A systematic analysis for the Global Burden of Disease Study, *Lancet*, 1923–1994, doi:10.1016/S0140-6736(18)32225-6,
715 2018.
- Strode, S. A., Rodriguez, J. M., Logan, J. A., Cooper, O. R., Witte, J. C., Lamsal, L. N., Damon, M., Van Aartsen, B., Steenrod,
S. D. and Strahan, S. E.: Trends and variability in surface ozone over the United States, *J. Geophys. Res.*, 120, 9020–9042,
doi:10.1002/2014JD022784, 2015.
- Strode, S. A., Ziemke, J. R., Oman, L. D., Lamsal, L. N., Olsen, M. A. and Liu, J.: Global changes in the diurnal cycle of surface
720 ozone, *Atmos. Environ.*, 199, 323–333, doi:10.1016/j.atmosenv.2018.11.028, 2019.
- Thompson, M. Lou, Reynolds, J., Cox, L. H., Guttorp, P. and Sampson, P. D.: A review of statistical methods for the
meteorological adjustment of tropospheric ozone, *Atmos. Environ.*, 35(3), 617–630, doi:10.1016/S1352-2310(00)00261-2, 2001.
- Travis, K. R., Jacob, D. J., Fisher, J. A., Kim, P. S., Marais, E. A., Zhu, L., Yu, K., Miller, C. C., Yantosca, R. M., Sulprizio, M.
P., Thompson, A. M., Wennberg, P. O., Crouse, J. D., St. Clair, J. M., Cohen, R. C., Laughner, J. L., Dibb, J. E., Hall, S. R.,
725 Ullmann, K., Wolfe, G. M., Pollack, I. B., Peischl, J., Neuman, J. A. and Zhou, X.: Why do models overestimate surface ozone
in the Southeast United States?, *Atmos. Chem. Phys.*, 16, 13561–13577, doi:10.5194/acp-16-13561-2016, 2016.
- Turner, M. C., Jerrett, M., Pope, C. A., Krewski, D., Gapstur, S. M., Diver, W. R., Beckerman, B. S., Marshall, J. D., Su, J.,
Crouse, D. L. and Burnett, R. T.: Long-Term Ozone Exposure and Mortality in a Large Prospective Study, *Am. J. Respir. Crit.*



Care Med., 193(10), 1134–1142, doi:10.1164/rccm.201508-1633oc, 2016.

730 U.S. EPA. Integrated science assessment for ozone and related photochemical oxidants. Office of Research and Development - National Center for Environmental Assessment- RTP. EPA/600/R-10/076F, 2013.

Van Dingenen, R., Dentener, F. J., Raes, F., Krol, M. C., Emberson, L. and Cofala, J.: The global impact of ozone on agricultural crop yields under current and future air quality legislation, *Atmos. Environ.*, 43, 604–618, doi:10.1016/j.atmosenv.2008.10.033, 2009.

735 van Donkelaar, A., Martin, R. V., Li, C. and Burnett, R. T.: Regional Estimates of Chemical Composition of Fine Particulate Matter Using a Combined Geoscience-Statistical Method with Information from Satellites, Models, and Monitors, *Environ. Sci. Technol.*, 53(5), 2595–2611, doi:10.1021/acs.est.8b06392, 2019.

Xing, J., Pleim, J., Mathur, R., Pouliot, G., Hogrefe, C., Gan, C.-M. and Wei, C.: Historical gaseous and primary aerosol emissions in the United States from 1990 to 2010, *Atmos. Chem. Phys.*, 13(15), 7531–7549, doi:10.5194/acp-13-7531-2013,

740 2013.

Yan, Y., Lin, J., Chen, J. and Hu, L.: Improved simulation of tropospheric ozone by a global-multi-regional two-way coupling model system, *Atmos. Chem. Phys.*, 16(4), 2381–2400, doi:10.5194/acp-16-2381-2016, 2016.

Yi, J. and Prybutok, V. R.: A neural network model forecasting for prediction of daily maximum ozone concentration in an industrialized urban area, *Environ. Pollut.*, 92(3), 349–357, doi:10.1016/0269-7491(95)00078-X, 1996.

745 Young, P. J., Naik, V., Fiore, A. M., Gaudel, A., Guo, J., Lin, M. Y., Neu, J. L., Parrish, D. D., Rieder, H. E., Schnell, J. L., Tilmes, S., Wild, O., Zhang, L., Ziemke, J. R., Brandt, J., Delcloo, A., Doherty, R. M., Geels, C., Heggin, M. I., Hu, L., Im, U., Kumar, R., Luhar, A., Murray, L., Plummer, D., Rodriguez, J., Saiz-Lopez, A., Schultz, M. G., Woodhouse, M. T. and Zeng, G.: Tropospheric Ozone Assessment Report: Assessment of global-scale model performance for global and regional ozone distributions, variability, and trends, *Elem. Sci. Anthr.*, 6(10), doi:10.1525/elementa.265, 2018.

750 Zhang, L., Jacob, D. J., Knipping, E. M., Kumar, N., Munger, J. W., Carouge, C. C., van Donkelaar, A., Wang, Y. X. and Chen, D.: Nitrogen deposition to the United States: distribution, sources, and processes, *Atmos. Chem. Phys.*, 12, 4539–4554, doi:10.5194/acp-12-4539-2012, 2012.

Zhang, Y., West, J. J., Mathur, R., Xing, J., Hogrefe, C., Roselle, S. J., Bash, J. O., Pleim, J., Gan, C.-M. and Wong, D. C.: Long-term trends in the PM_{2.5}- and O₃-related mortality burdens in the United States under emission reductions from 1990 to

755 2010, *Atmos. Chem. Phys.*, 18, 15003–15016, doi:10.5194/acp-18-15003-2018, 2018.

Zheng, B., Tong, D., Li, M., Liu, F., Hong, C., Geng, G., Li, H., Li, X., Peng, L., Qi, J., Yan, L., Zhang, Y., Zhao, H., Zheng, Y., He, K. and Zhang, Q.: Trends in China's anthropogenic emissions since 2010 as the consequence of clean air actions, *Atmos. Chem. Phys.*, 18(19), 14095–14111, doi:10.5194/acp-18-14095-2018, 2018.



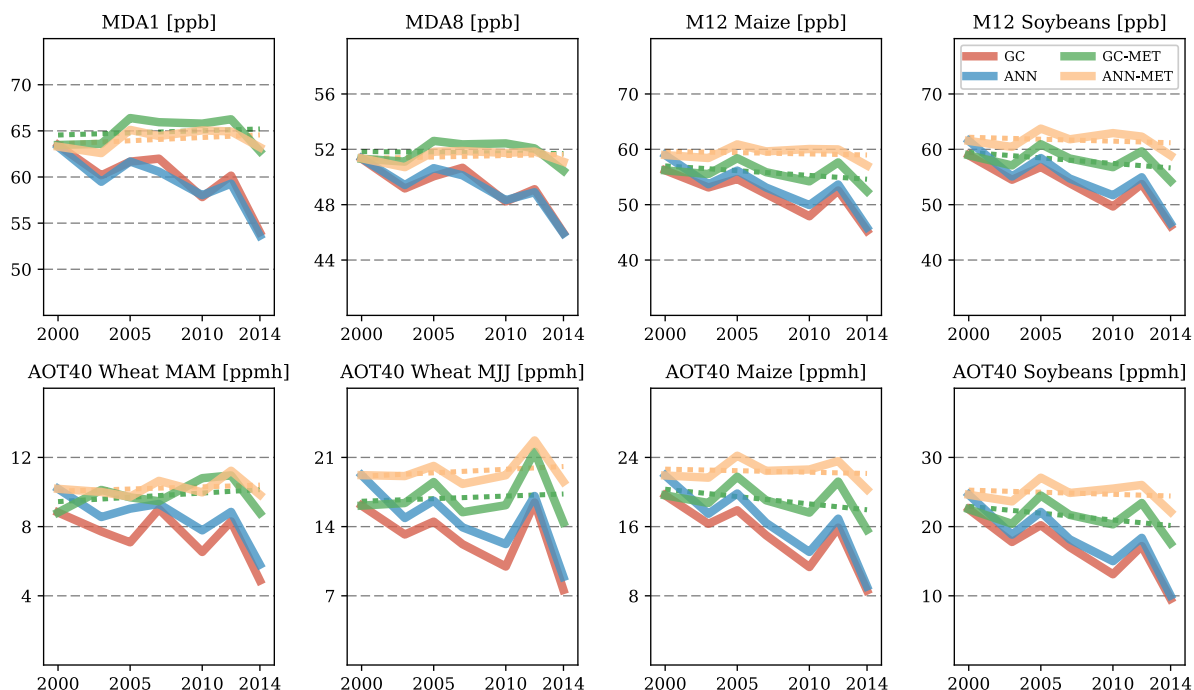
760 **Table 1: Daily-level training, validation, and testing performance metrics (RMSE) of the ANN using GEOS-Chem sampled data at TOAR locations compared to a multiple-linear regression model.**

Dataset	MDA1		MDA8		M12		AOT40	
	ANN [ppb]	MLR [ppb]	ANN [ppb]	MLR [ppb]	ANN [ppb]	MLR [ppb]	ANN [ppbh]	MLR [ppbh]
Training	6.91	10.69	6.62	10.32	6.48	9.93	62.83	98.15
Validation	7.16	10.60	6.95	10.55	6.68	9.74	64.97	97.48
Testing	7.09	10.50	6.83	10.18	6.86	10.03	66.68	100.43

765

Table 2: Daily-level training, validation, and testing performance metrics (RMSE) of the ANN using TOAR observations compared to a multiple-linear regression model.

Dataset	MDA1		MDA8		M12		AOT40	
	ANN [ppb]	MLR [ppb]	ANN [ppb]	MLR [ppb]	ANN [ppb]	MLR [ppb]	ANN [ppbh]	MLR [ppbh]
Training	9.25	13.02	8.24	11.65	7.89	10.90	55.69	78.50
Validation	9.36	13.26	8.24	11.43	8.06	11.16	56.22	76.98
Testing	9.39	13.08	8.23	11.56	7.87	10.76	57.13	78.55



770

Figure 1: Red - GEOS-Chem simulated values of all metrics. Blue - ANN predictions using daily samples of the GEOS-Chem simulations at all available monitoring stations. Green - Meteorological trend simulated by GEOS-Chem with all input frozen at 2000 levels, with the exception of meteorological variables. Yellow - ANN prediction of the GC-MET (green) trend using the neural networks trained with the original (i.e. blue) data.

775

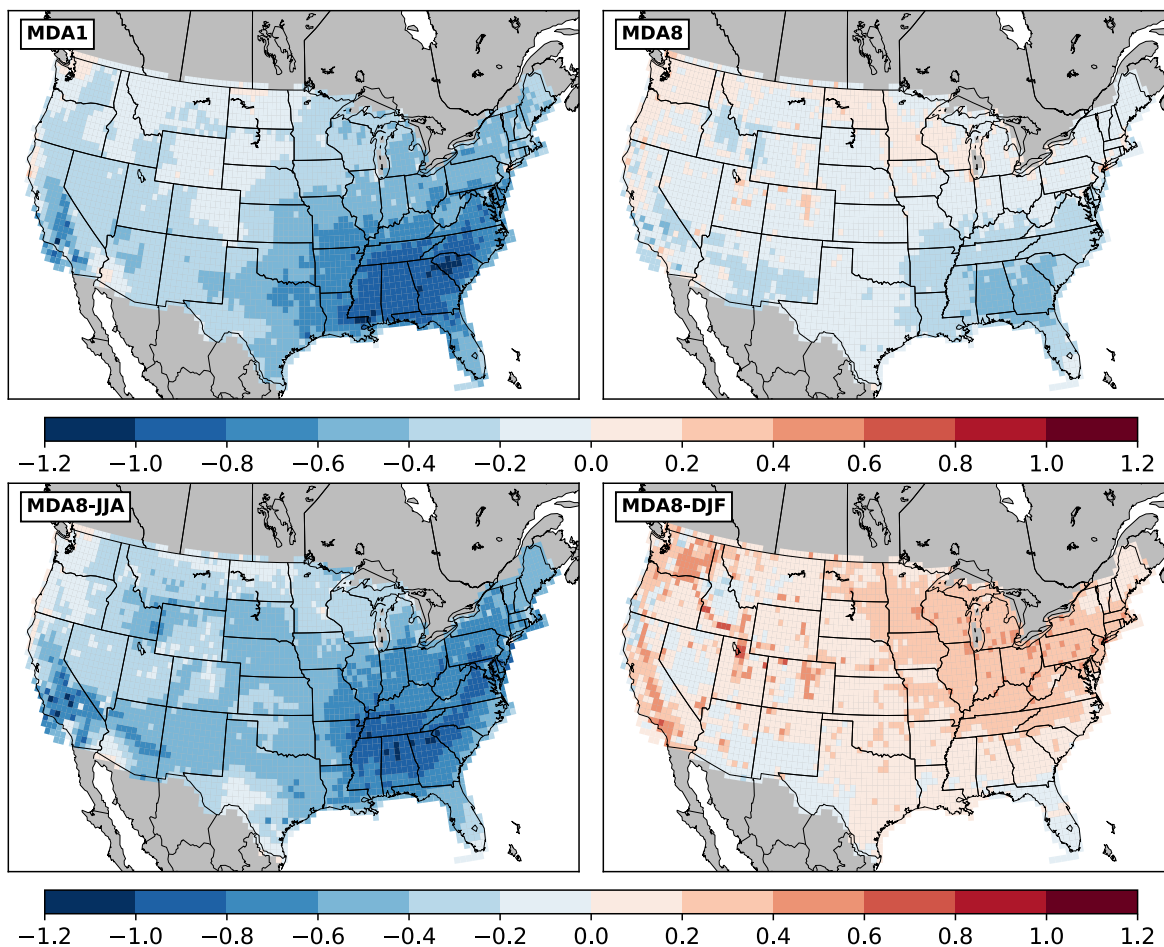
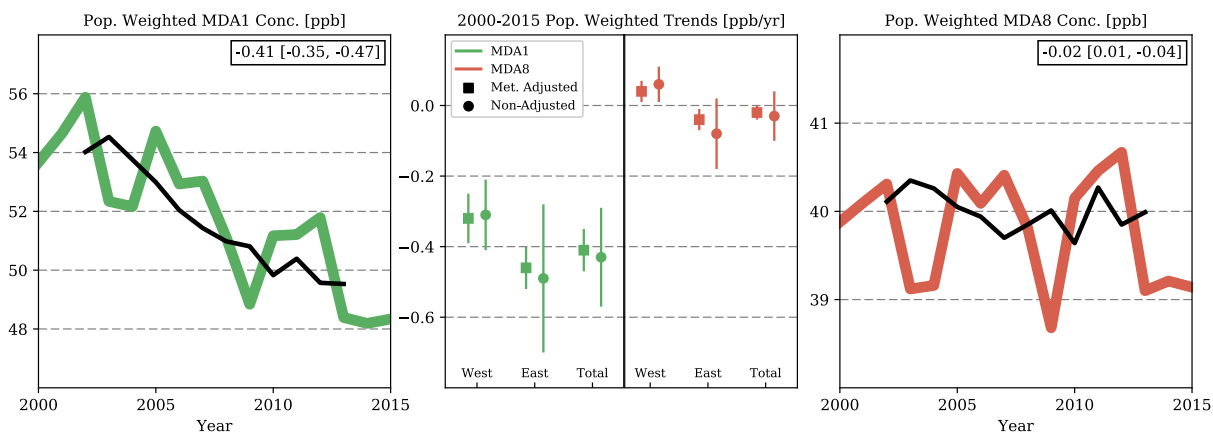


Figure 2: Top row - Trends of the MDA1 (left; ppb/yr) and MDA8 (right; ppb/yr) health-metrics from 2000-2015. Bottom row - Trends of the MDA8-JJA (summer month; left; ppb/yr) and MDA8-DJF (winter month; right; ppb/yr) from 2000-2015. The p-values from these trends can be found in Fig. S5.



785 **Figure 3: Left - Population-weighted exposure concentrations of the MDA1 human-health metric from 2000-2015. The meteorologically adjusted trend is in black with the slope in the inset. Middle - 2000-2015 population-weighted trends [ppb/yr] of the MDA1 (green) and MDA8 (red) metrics. The west/east divide is made along the 95W meridian and the whiskers span the 95% confidence interval. Right - Population-weighted exposure concentrations of the MDA8 human-health metric from 2000-2015. The meteorologically adjusted trend is in black with the slope in the inset. Tabulated values of these plots can be found in Table S2 and S4.**

790

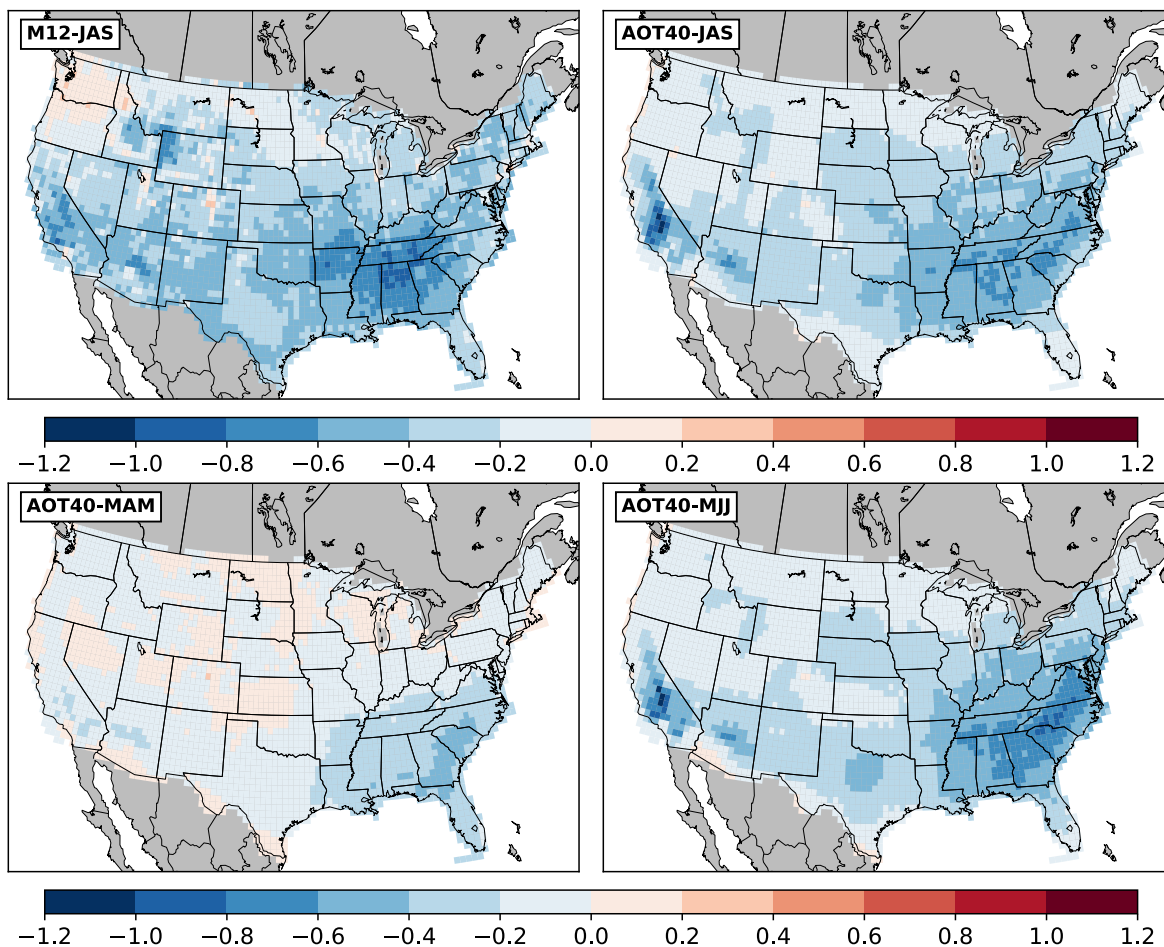
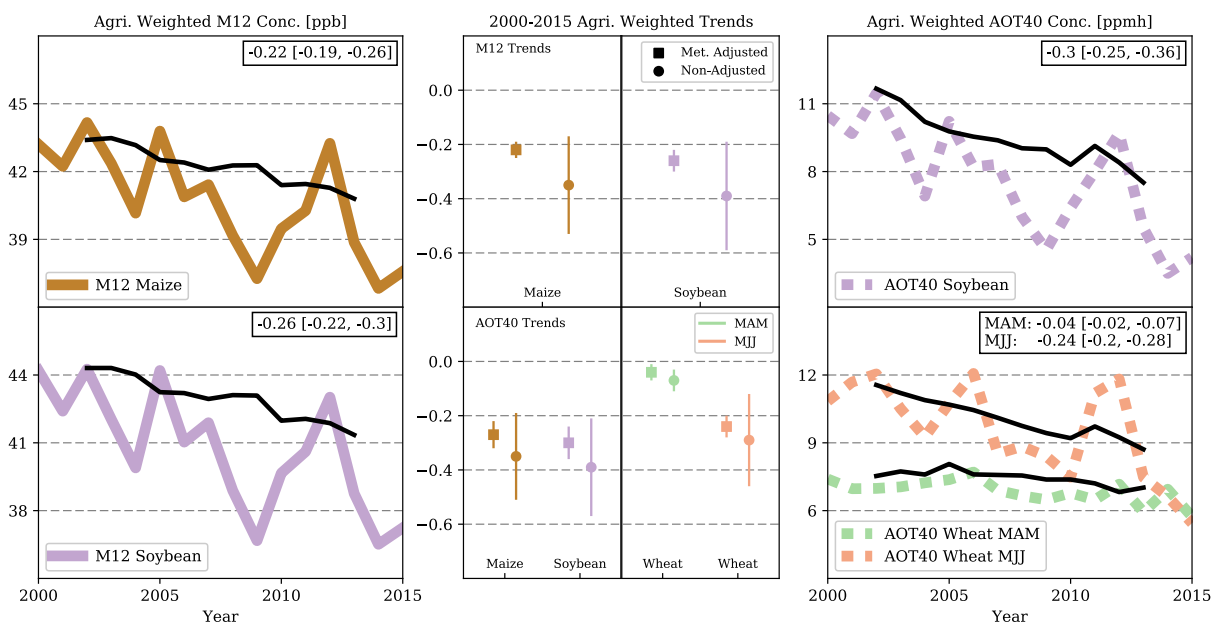


Figure 4: Trends of the M12 (top left; ppb/yr) and AOT40 (top right and bottom; ppmh/yr) agriculture-metrics from 2000-2015. Note: JAS = July-September; MAM = March-May; MJJ = May-July. The p-values from these trends can be found in Fig. S6.



795

Figure 5: Left - Agriculture-weighted exposure concentrations of the M12 agriculture metrics from 2000-2015. The meteorologically adjusted trend of each metric is in black with the slope in the inset. Middle - 2000-2015 agriculture-weighted trends (ppb/yr for M12, ppmh/yr for AOT40) of the M12 and AOT40 metrics. The whiskers span the 95% confidence interval. Right - Agriculture-weighted exposure concentrations of the AOT40 agriculture metrics from 2000-2015. The meteorologically adjusted trend of each metric is in black with the slope in the inset. Note: variable averaging periods are considered, reflecting differences in crop harvest seasons. Tabulated values of the left and right plots can be found in Table S3 and S4.

800

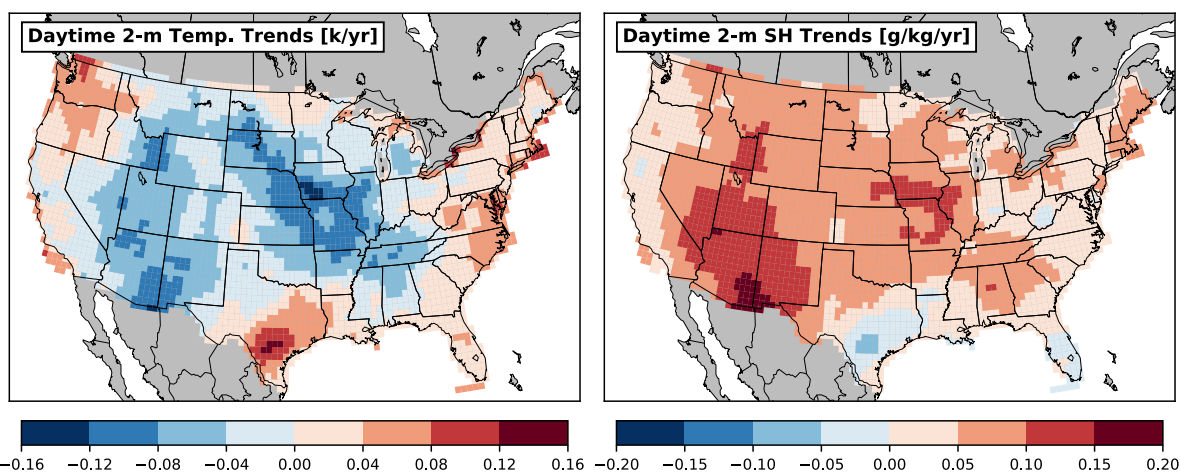
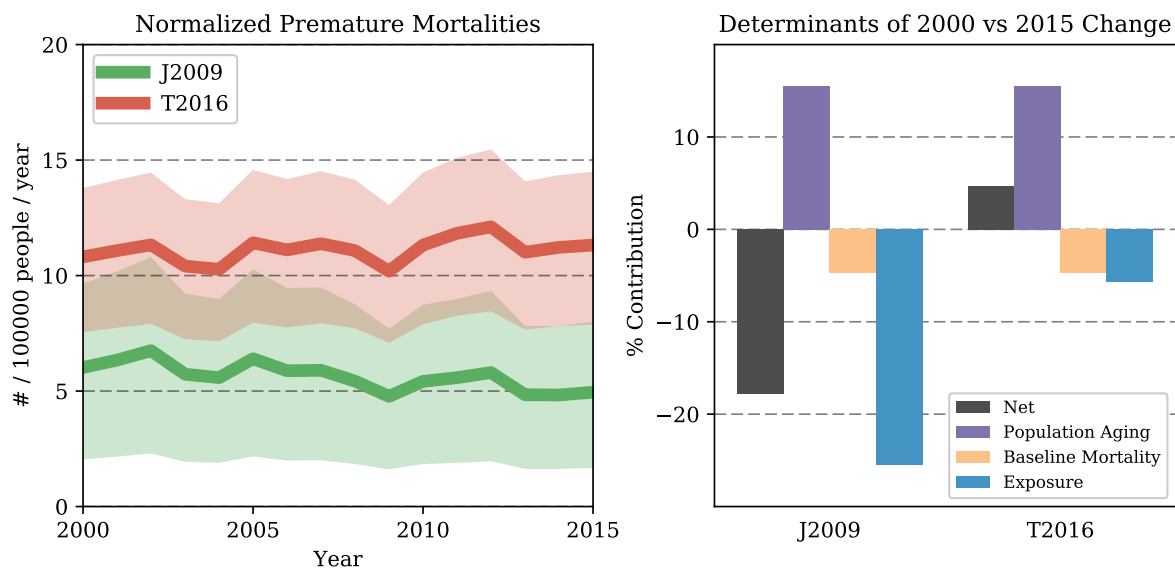
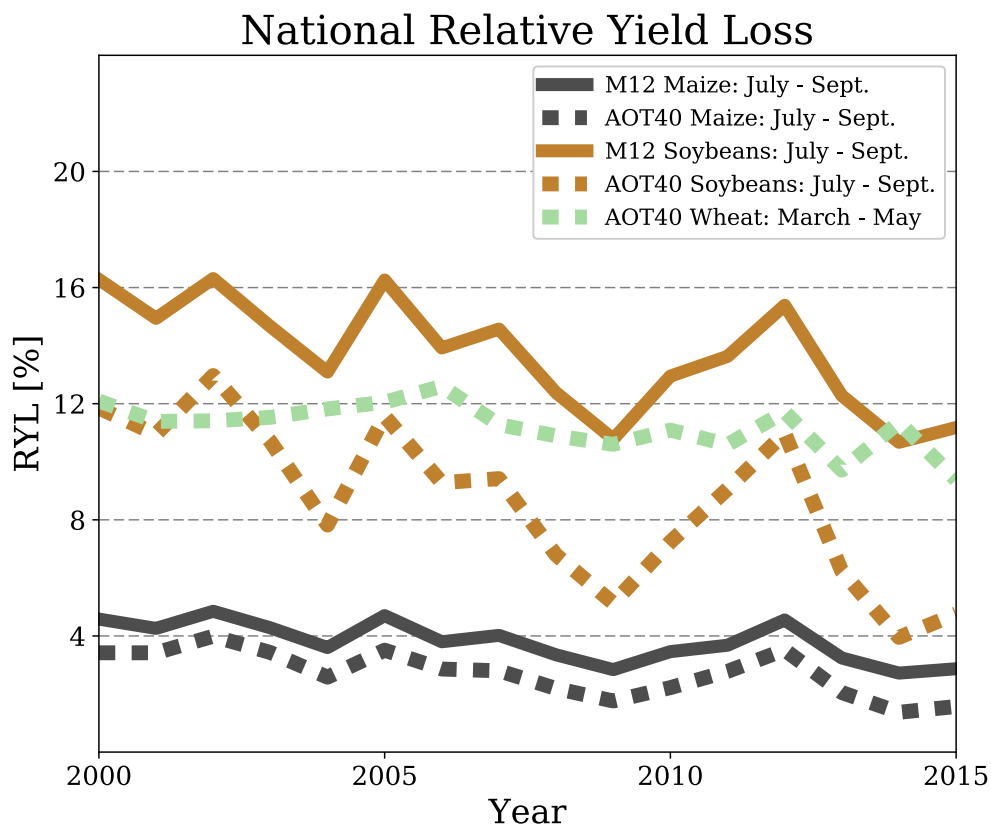


Figure 6: Annual trends in the daytime 2-meter temperature and daytime 2-meter specific humidity from 2000-2015.



810 **Figure 7:** Left - Annual estimates of normalized premature mortalities (# per 100,000 people per year) attributable to long-term O₃ exposure using the MDA1 and MDA8 averaging metrics and exposure-response function from J2009 and T2016, respectively. Shaded region reflects confidence interval reported in each underlying epidemiological study. Right - 2000 vs. 2015 percent contributions of population aging, changing baseline mortality rates, and long-term O₃ exposure to net normalized premature mortalities using the MDA1 and MDA8 averaging metrics and exposure-response function from J2009 and T2016, respectively. Tabulated values of the left plot can be found in Table S5.



815

Figure 8: Estimates of the national relative yield loss for a variety of commercial crops using ANN calculated exposure metrics. Tabulated values of this plot can be found in Table S5.